J. Fluid Mech. (2004), *vol.* 520, *pp.* 157–186.
DOI: 10.1017/S002211200400134X Printed in the United Kingdom

Three-dimensional analysis of the unidirectional oscillatory flow around a circular cylinder at low Keulegan–Carpenter and β numbers

By D. NEHARI[1], V. ARMENIO[2]† AND F. BALLIO[3]

[1]Département de Génie Mécanique, Université de Mostaganem, Mostaganem, Algeria
[2]Dipartimento di Ingegneria Civile, Università degli Studi di Trieste, Trieste, Italy
[3]DIIAR, Politecnico di Milano, Milano, Italy

(Received 4 November 2003 and in revised form 26 July 2004)

In this paper, the oscillating flow around a circular cylinder is investigated numerically using both a three-dimensional and a two-dimensional model. Two important three-dimensional regimes of the Tatsuno & Bearman (*J. Fluid Mech.* vol. 211, 1990, p. 157) map are investigated: the asymmetric transverse-street regime D, and the double-pair diagonal regime F. The Stokes number is held constant ($\beta = 20$) and the Keulegan–Carpenter number and the Reynolds number changed so that they match the conditions of these two regimes.

The cross-sectional vortex streets (V-pattern in regime D and diagonal pattern in regime F) appear to be unstable, and switching from a pattern to its mirror-image mode occurs during the simulation. This switching is related to a two-dimensional instability in the flow field; this phenomenon can be reproduced by pure two-dimensional simulations.

Three-dimensionality in the flow field always appears after the asymmetric vortex pattern has fully developed. The main effect of three-dimensionality in the flow field appears to be a rotation (circumferential effect) along the axial direction of the main sectional vortex patterns and a time delay along this axis of the switching from a two-dimensional mode to its mirror-image. These features contribute to generation of the three-dimensional sinuous S-mode as defined by Yang & Rockwell (*J. Fluid Mech.* vol. 460, 2002, p. 93).

The three-dimensionality of the vorticity field affects the dynamic loads induced on the cylinder. The longitudinal component of the force acting on the cylinder appears to be weakly affected by three-dimensional effects, and so does its distribution in the axial direction. This finding explains why the results of two-dimensional simulations often agree fairly well with the data from laboratory experiments. Conversely, the transversal force appears to be significantly affected by the three-dimensional flow field, which suggests that an accurate numerical prediction requires the use of three-dimensional numerical models.

Finally, a simplified conceptual model explains why the axial variation of the sectional transversal force always appears to be much larger than that of the corresponding longitudinal one. The model also explains why two-dimensional simulations tend to underpredict the r.m.s. value of the longitudinal force and to overpredict that of the transversal force, compared to the data from three-dimensional studies.

† Author to whom correspondence should be addressed: armenio@dic.units.it

1. Introduction

The study of the oscillating flow around circular cylinders is of importance in off-shore engineering because it is an idealized representation of the wave-induced loads on cylindrical structures (Bearman 1997). The flow field depends on two non-dimensional parameters: the Keulegan–Carpenter number and the Reynolds number. The Keulegan–Carpenter number is $KC = U_{max}T/D$, where U_{max} is the maximum velocity of the external oscillating flow, T is the period of oscillation and D is the diameter of the cylinder, and it is the ratio between the time scale T imposed by the flow and the inertial time scale D/U_{max}. The Reynolds number, $Re = U_{max}D/\nu$ (where ν is the fluid kinematic viscosity), is the usual ratio between the viscous time scale D^2/ν and the inertial time scale D/U_{max}. A parameter often used for the characterization of the flow field is the Stokes number $\beta = Re/KC = D^2/T\nu$. Note that the Stokes number is independent of the velocity of the outer flow U_{max} and can be regarded as the ratio between the viscous time scale and that of the external oscillating motion T.

The resulting flow field is complex and characterized by vortex shedding, the pattern of which may change dramatically according to the magnitude of the above parameters. Vortex shedding tends to be asymmetric, thus generating a transversal force whose first mode of oscillation is a fraction of the period T of the imposed motion.

The flow field around a circular cylinder in oscillatory motion in a fluid at rest has been studied in the past. Several flow regimes have been detected, each of them characterized by repeatable vortex patterns. Williamson (1985) experimentally investigated a wide range of KC for very large values of the parameter β, focusing on vortex shedding in the two-dimensional plane containing the cross-section of the cylinder, and measuring the forces induced on the cylinder itself. Specifically, depending on KC, Williamson (1985) has observed pairing of attached vortices, a transverse street of vortices, a double pair, three pairs, and four pairs of vortices.

By visualizing the flow field around a circular cylinder oscillating in a tank of water, Tatsuno & Bearman (1990, referred to herein as TB90) identified eight different flow regimes (A^*, A, B, C, D, E, F, and G), most of which resulted in three-dimensional flow patterns, depending on the two parameters KC and Re, or equivalently, on KC and β (figure 1). Two-dimensional symmetric regimes were identified as A^* and A respectively in the range of very small KC and large β, and large KC and small β. At intermediate Stokes numbers an increase in KC gave rise to asymmetry in vortex shedding and the appearance of a periodical transversal force (regimes B to G). These regimes were also accompanied by three-dimensional effects, in that organized vortex structures were observed to develop along the direction of the cylinder's axis. Vortex patterns in the cross-sectional planes matched those identified by Williamson (1985). Two-dimensional as well as three-dimensional vortex structures were clearly visualized and identified in TB90, although their magnitude was not evaluated. The axial average wavelength of such vortex structures was found to vary between $0.8D$ and $6D$ depending on the regime of motion depicted in figure 1.

The three-dimensional modes developing along a cylinder in oscillatory motion have been quantified in a recent paper by Yang & Rockwell (2002, referred to herein as YR02) for $\beta = 73$ and small to moderate values of KC, in which results were presented for $4.5 < KC < 21.4$. Referring to figure 1, the YR02 experiments were carried out in regimes B, E and G, which are asymmetric and three-dimensional. Unlike most of the investigations cited above (carried out in unidirectional flow) the experiments by YR02 were performed in a wavy flow characterized by a elliptic trajectory of the

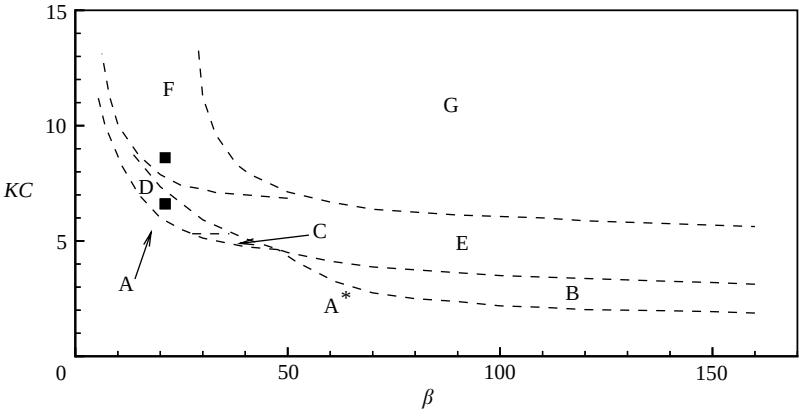

FIGURE 1. Map by Tatsuno & Bearman (1990) identifying the different flow regimes in the KC–β plane. A: symmetric with vortex shedding, two-dimensional; A*: symmetric and attached, two-dimensional; B: longitudinal vortices, three-dimensional streaked flow; C: rearrangement of large vortices, three-dimensional; D: transverse street, three-dimensional; E: transverse street with irregular switching, three-dimensional; F: diagonal double-pair, three-dimensional; G: transverse vortex street, three-dimensional. The squares indicate the cases investigated here.

fluid particles, which decreased in size and tended to be increasingly elongated in the horizontal direction with increasing depth. YR02 found that either a sinuous S-mode or an unidirectional U-mode may develop along the axial direction†, as also detected in the visual analysis by Obasaju, Bearman & Graham (1988) for $\beta > 100$. Small-scale axial modes, with non-dimensional characteristic wavelength $1 < \lambda = \lambda_d/D < 4.5$ (λ_d is the dimensional wavelength), were found for small values of KC, whereas for $KC \geqslant 10$ large-scale modes were detected with $10 < \lambda < 110$ (see YR02).

Two-dimensional numerical investigations of the oscillating flow around a circular cylinder have been performed by Justusen (1991) and by Dutsch *et al.* (1998). The aim of these studies was to reproduce the main features of the vortex shedding occurring in the above-mentioned flow regimes and to evaluate the time evolution of the forces that act on the cylinder. Justusen (1991) simulated most of the two-dimensional regimes defined by Williamson (1985), obtaining generally good agreement between numerical results and experimental data, although he stressed the need for a more realistic three-dimensional model. Dutsch *et al.* (1998) used the two-dimensional Navier–Stokes equations and also performed laboratory experiments for the investigation of three different flow regimes of the map of TB90, namely regimes A (symmetric), F (diagonal, double-pair vortex shedding) and E (transverse street). Overall they obtained good agreement between experimental results and corresponding numerical predictions for the velocity field and force coefficients. Further computations for the Stokes number $\beta = 35$ were carried out mainly in order to compare force coefficients with the experimental results of Kuhtz (1981). The coefficients derived from the

† According to YR02, the sinuous S-mode corresponds to a sinuous form of the instantaneous velocity vectors and to a multiple zero-crossing of the near-body crossflow velocity $w(y)$ along the y-axis in the plane $z = 0$. Conversely, the unidirectional U-mode is characterized by the unidirectional movement of the near-body wake and thus by the fact that the near-body crossflow velocity $w(y)$ maintains its sign along the y-axis in the plane $z = 0$. For the frame of reference see figure 2.

numerical predictions were found to be in good agreement with those of the experiments, although some small differences, attributed to three-dimensional effects, were found.

A three-dimensional flow field is an inherent characteristic of the oscillating flow around a cylinder, even in the presence of unidirectional forcing. Nonetheless, to the best of our knowledge, the literature contains no three-dimensional numerical solutions to be compared with experimental observations of the three-dimensional vorticity field and force distribution. For example, the three-dimensional numerical study by Zhang & Dalton (1999) focused on the viscous transition from two to three dimensions in the wake of the cylinder (the Honji instability, Honji 1981).

To summarize:

(i) Extensive experimental investigations have examined the different flow regimes occurring in the planes (KC, Re) or (KC, β) by flow visualization, and measurements have been made of the longitudinal and transversal forces that arise in the above regimes.

(ii) two-dimensional computations have been performed, in order to reproduce two-dimensional vortex patterns visualized in the experimental investigations and to evaluate the longitudinal and transversal forces in several flow regimes.

The three-dimensional features of the phenomenon have not been thoroughly investigated; their effects on the evolution of the forces, as well as how and to what extent three-dimensional modes affect the distribution of the sectional in-line and transversal loads, are still not completely understood (see for example the survey by Bearman 1997).

The rationale of the present study is as follows: we intend to explore two important regimes of the TB90 map, the purpose being to reproduce the three-dimensionality of the flow field and to quantify its effects on the magnitude and on the axial modulation of the forces induced over the cylinder.

The investigation is performed numerically, solving both the three-dimensional and the two-dimensional unsteady Navier–Stokes equations. A unidirectional flow field oscillating sinusoidally in time is considered; the Stokes number is held constant ($\beta = 20$); KC and Re are such that two three-dimensional regimes, namely D and F, of the map of TB90 are explored (see figure 1). Regime D is a transverse-street one, whereas F is a double-pair diagonal regime. For each regime we analyse the evolution of the vorticity field and its relationship with the induced loads.

To the best of our knowledge, this is the first investigation that reproduces the three-dimensional vortex structures visualized by TB90 by means of numerical simulations and quantifies their effects on the axial distribution of the force components. It is also the first study which compares the results of three-dimensional simulations with those of equivalent two-dimensional simulations.

The paper is organized as follows: § 2 contains the mathematical model, and gives a brief description of the algorithm used for the integration of the governing equations and validation tests. Sections 3 and 4 contain the results for the two regimes investigated. Concluding remarks are given in § 5.

2. The problem formulation

We consider a circular cylinder placed in a fluid that undergoes a sinusoidal oscillation with given frequency and amplitude, in laminar-flow conditions. We use the primitive-variable formulation of the non-dimensional, unsteady and

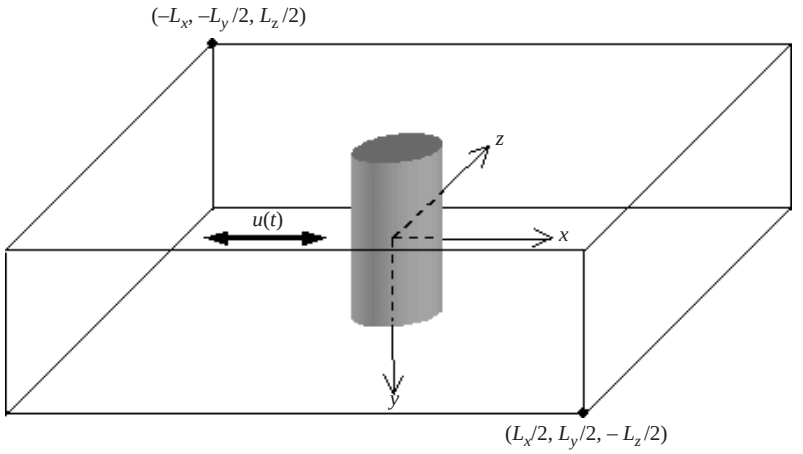

FIGURE 2. Schematic of the physical problem investigated.

three-dimensional Navier–Stokes (NS) equations written in curvilinear coordinates:

$$\frac{\partial U^m}{\partial \xi^m} = 0, \tag{2.1}$$

$$\frac{1}{KC}\frac{\partial J^{-1}u_i}{\partial t} + \frac{\partial U^m u_i}{\partial \xi^m} = -\frac{\partial}{\partial \xi^m}\left(J^{-1}\frac{\partial \xi^m}{\partial x_i}p\right) + \frac{1}{Re}\frac{\partial}{\partial \xi^m}\left(G^{mn}\frac{\partial u_i}{\partial \xi^n}\right) - J^{-1}B_i. \tag{2.2}$$

In (2.1) and (2.2) u_i represents the i-component of the velocity field made dimensionless with the maximum amplitude of the streamwise velocity during the cycle of oscillation U_{max}, $x_i = x_{d,i}/D$ (hereafter index d refers to dimensional quantities) with $i = 1, 2, 3$ or x, y, z are, respectively, the non-dimensional streamwise, axial and transversal coordinates; t is the time made non-dimensional with the period T and $p = (p_d - p_0)/\rho U_{max}^2$ is the non-dimensional pressure where p_0 is a reference value. Further, ξ^m $(m = 1, 2, 3)$ represents the coordinate directions in the computational space; J^{-1} is the inverse of the Jacobian of the transformation from the physical domain to the computational one; $U^m = J^{-1}(\partial \xi^m/\partial x_j\ u_j)$ is the non-dimensional contravariant flux through the plane $\xi^m = \text{const}$, and $G^{mn} = J^{-1}(\partial \xi^m/\partial x_j)(\partial \xi^n/\partial x_j)$ is the mesh skewness tensor. In (2.2), B_i is the non-dimensional pressure gradient that drives the oscillating flow:

$$B_i = -\frac{2\pi}{KC}\delta_{i1}\cos(2\pi t), \tag{2.3}$$

where δ is the Kronecker symbol. This term is a body force that must be added when studying the oscillatory motion of a cylinder in a fluid otherwise at rest, using a frame of reference attached to the cylinder: it corresponds to the forcing term of equation (2.6) in Dutsch *et al.* (1998). It is easy to show that the imposed pressure gradient (2.3) produces a non-dimensional outer velocity $u(t) = \sin(2\pi t)$. Figure 2 shows a schematic of the problem under investigation together with the frame of reference that has its origin at the centre of the cylinder.

2.1. *The numerical method*

Equations (2.1) and (2.2) are integrated numerically using the finite-difference non-staggered-grid fractional-step algorithm developed by Zang, Street & Koseff (1994). The Adams–Bashforth technique is used for the time advancement of the convective

terms and of the off-diagonal diffusive terms that arise in non-orthogonal grids ($G^{mn} \neq 0$ for $m \neq n$), whereas the diagonal diffusive terms are treated implicitly using the Crank–Nicolson technique. The spatial derivatives are evaluated using second-order centred finite differences. A multigrid technique is employed to solve the pressure equation. The algorithm is overall second-order accurate both in time and in space.

2.2. *Boundary and initial conditions*

For a circular cylinder in oscillatory motion in a fluid at rest, the experiments reported in TB90 have shown that most three-dimensional flow regimes are characterized by three-dimensional vortex structures that repeat periodically along the axial direction. The wavelength of the three-dimensional vortex structures has been observed to range between 0.5 and 6 diameters. Furthermore, the experimental study by YR02 has shown that for values of $KC < 10$, small-scale three-dimensional vortex structures can be observed, with values of wavelength similar to those recorded by TB90.

It follows that, for such regimes, periodic conditions can be used along the y-direction, provided that the length of the cylinder is sufficient to contain the observed structures. Obviously, an appropriate length of the cylinder must be chosen, being a compromise between the number of grid cells to be placed along the axial direction and the length of the cylinder. Considering that (i) we were interested in values of KC smaller than 10, characterized by the presence of small-scale wavelength as discussed above, and (ii) that a well-resolved three-dimensional simulation of the oscillating flow around a very long cylinder (say $L_y/D \sim 20$ or more) could not be carried out because of prohibitive computational efforts, we decided to use a cylinder length equal to 12 diameters. This enabled us to correctly simulate the small-scale three-dimensional modes discussed above.

Finally, periodicity was imposed in the transversal and in the longitudinal directions. As regards the length of the domain in the x-direction, a preliminary analysis carried out using different lengths and a short cylinder ($L_y = 4$) showed that in both regimes investigated the vorticity components decay within 7 to 8 diameters along the x-axis, hence the length of the domain chosen was equal to 26 diameters. In the z-direction the width of the domain chosen was equal to 14 diameters; we checked that in all cases investigated in the present paper, the vorticity components decay to negligible values within 5 diameters along the z-direction. Finally, no-slip conditions were applied on the surface of the cylinder. The initial condition in each case was a state of rest.

2.3. *Grid generation*

We used an H-grid topology such that the physical domain was a rectangular box that contained the cylinder, doing so in conjunction with a version of the code able to handle a singularity line within the computational box. This line was transformed into two halves of the cylinder in the physical domain. The domain was symmetric with respect to the longitudinal plane $z = 0$ and to the transversal plane $x = 0$. The grid is generated using the technique of Sorenson (1980) which ensures grid orthogonality at the boundaries and allows specification of the spacing of the first coordinate surface off the body. In our study, this technique enabled us to generate high-quality grids, with coordinate lines orthogonal to the boundary surfaces including the body surface, and closely clustered near the body surface. The grid was uniform in the axial (y) direction. An example of the grid topology used for the planes $y = const$ is given in figure 3.

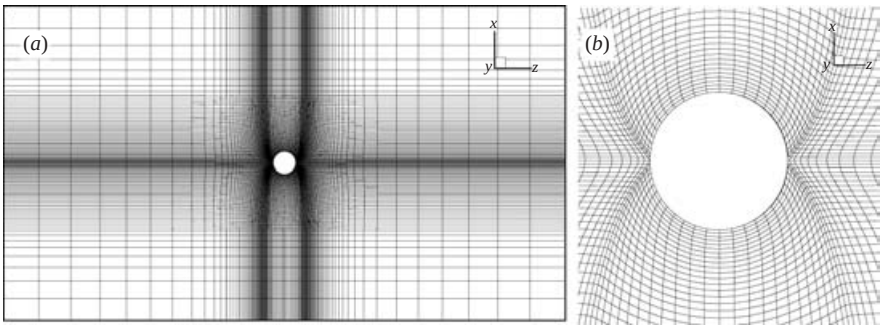

FIGURE 3. Typical H-grid used in the computations. The grid is for the (x, z)-planes: (a) overall view; (b) near-cylinder view.

2.4. *Evaluation of the vorticity field and of the time-dependent forces*

Analysis of the instantaneous vorticity field can help to identify the vortex structures that evolve in the flow field. The vorticity field can be expressed by means of the Cartesian components as

$$\omega_i = \frac{\partial u_k}{\partial x_j} - \frac{\partial u_j}{\partial x_k}. \tag{2.4}$$

The derivatives in (2.4) were evaluated at the centre of the grid cells by means of second-order-accurate centred finite differences, and using the transformation relationships between the physical coordinates and the computational one, $\partial u_i/\partial x_j = (\partial u_i/\partial \xi^m)(\partial \xi^m/\partial x_i)$. Note that the vorticity components were made non-dimensional with U_{max}/D.

The time-dependent velocity and the pressure distributions obtained in the simulations were used to evaluate the forces acting on the cylinder. In particular, after neglecting the component of the force along the axis of the cylinder, because it is very small and not relevant to the purpose of the study, the total non-dimensional force could be decomposed into the longitudinal (x) component F_x and the transversal (z) one F_z:

$$F_x = \frac{1}{\rho U_{max}^2 D L_y}\left[-\int_{Sc} p_d \boldsymbol{n}\cdot\boldsymbol{i}\,\mathrm{d}s - \int_{Sc} \rho\nu \frac{\partial u_\tau}{\partial n}\boldsymbol{s}\cdot\boldsymbol{i}\,\mathrm{d}s\right], \tag{2.5}$$

$$F_z = \frac{1}{\rho U_{max}^2 D L_y}\left[-\int_{Sc} p_d \boldsymbol{n}\cdot\boldsymbol{k}\,\mathrm{d}s - \int_{Sc} \rho\nu \frac{\partial u_\tau}{\partial n}\boldsymbol{s}\cdot\boldsymbol{k}\,\mathrm{d}s\right], \tag{2.6}$$

where $\boldsymbol{i}$ and $\boldsymbol{k}$ are respectively the unit vectors in the streamwise and transversal directions, $\boldsymbol{n}$ and $\boldsymbol{s}$ are respectively the unit vectors in the normal and tangential directions over the body surface, $\mathrm{d}s$ is the elementary surface, Sc is the surface of the cylinder, $(\partial u_\tau/\partial n)$ is the dimensional shear at the surface of the cylinder and p_d is the dimensional pressure. The forces of (2.5) and (2.6) consist of a pressure and a shear contribution and they were evaluated at each time step during the computations. We also defined the non-dimensional longitudinal $F_x^s(y)$ and transversal $F_z^s(y)$ sectional forces. These were obtained in like manner to those of (2.5) and (2.6) except that the surface of integration extended from y to $y + \Delta y$. They represented the force components acting on a strip of cylinder of axial length Δy. These forces are made non-dimensional with $\rho U_{max}^2 D \Delta y$.

	three-dimensional	two-dimensional ($\omega-\psi$)	Dutsch *et al.* (1998) (coarse)	Dutsch *et al.* (1998) (fine)
C_m	2.47	2.43	2.45	2.45
C_D	2.13	2.10	2.10	2.09

TABLE 1. Morison's coefficients obtained respectively with the three-dimensional code, with the two-dimensional (ω–ψ) code, and with the two-dimensional coarse-grid ($n_{circ}=96$) and fine-grid ($n_{circ}=384$) simulations of Dutsch *et al.* (1998) in regime A, $KC=5$, $\beta=20$, $Re=100$.

2.5. *Validation*

The original version of the computer code employed in our analysis has been extensively validated in the past and widely used to investigate turbulent flow fields (see for example Armenio & Piomelli 2000; Falcomer & Armenio 2002; Armenio & Sarkar 2002). In particular, tests on the conservation properties of the algorithm (Armenio & Piomelli 2000), have shown that it is conservative at the second order for mass, momentum and kinetic energy. This yields good results using a moderate number of grid cells. Validation tests were conducted to evaluate the number of grid cells to be placed in the (x, z)-planes needed for accurate evaluation of the forces on the body. We performed the tests in regime A, with $KC=5$, $\beta=20$ which give $Re=100$, since the available experimental results refer to this case. Specifically, the test were carried out using $L_x=18$, $L_y=1$, $L_z=5$ and respectively $72\times8\times64$ points in the x-, y- and z-directions (with 48 grid points placed along the circumference of the cylinder). A two-dimensional simulation was also performed for such case using a computer code which solved the vorticity stream–function (ω–ψ) formulation of the NS equations in polar coordinates for an isolated cylinder in an oscillatory flow. In this case, the equations were numerically integrated using a mixed spectral–finite difference method and an explicit low-storage third-order Runge–Kutta time-marching scheme (Pentek, Kadtke & Pedrizzetti 1998). The two-dimensional (ω–ψ) simulation was carried out using respectively 32 and 128 points distributed along the circumferential and the radial directions.

Figure 4 shows a comparison between the in-line and the transversal components of the velocity field measured in the experiments by Dutsch *et al.* (1998) and those computed with our three-dimensional model. The comparison was performed at different phase positions t_p of the cycle near the surface of the cylinder (note that $t_p=(t-N_cT)/T$ where N_c is the cycle of oscillation and $N_cT<t<(N_c+1)T$). The velocity field appears to be very well predicted by our computational model and the agreement between the results of the two-dimensional code and those of the three-dimensional code is very good. The inertia and drag coefficients of the Morison equation calculated using the time history of the force obtained with the three-dimensional model and that of the two-dimensional model were compared with those obtained by Dutsch *et al.* (1998) in two-dimensional simulations. The comparison is reported in table 1. Additional tests were carried out in regime D and regime F in order to determine the number of grid cells that will yield accurate results in terms of vorticity field and force components. In particular, tests were carried out which compared the results of the three-dimensional model with those of the two-dimensional (ω–ψ) model in the two-dimensional regime (before the three-dimensional motion develops); an additional re-griding test was performed in order to determine the number of grid cells in the axial direction needed to ensure accuracy.

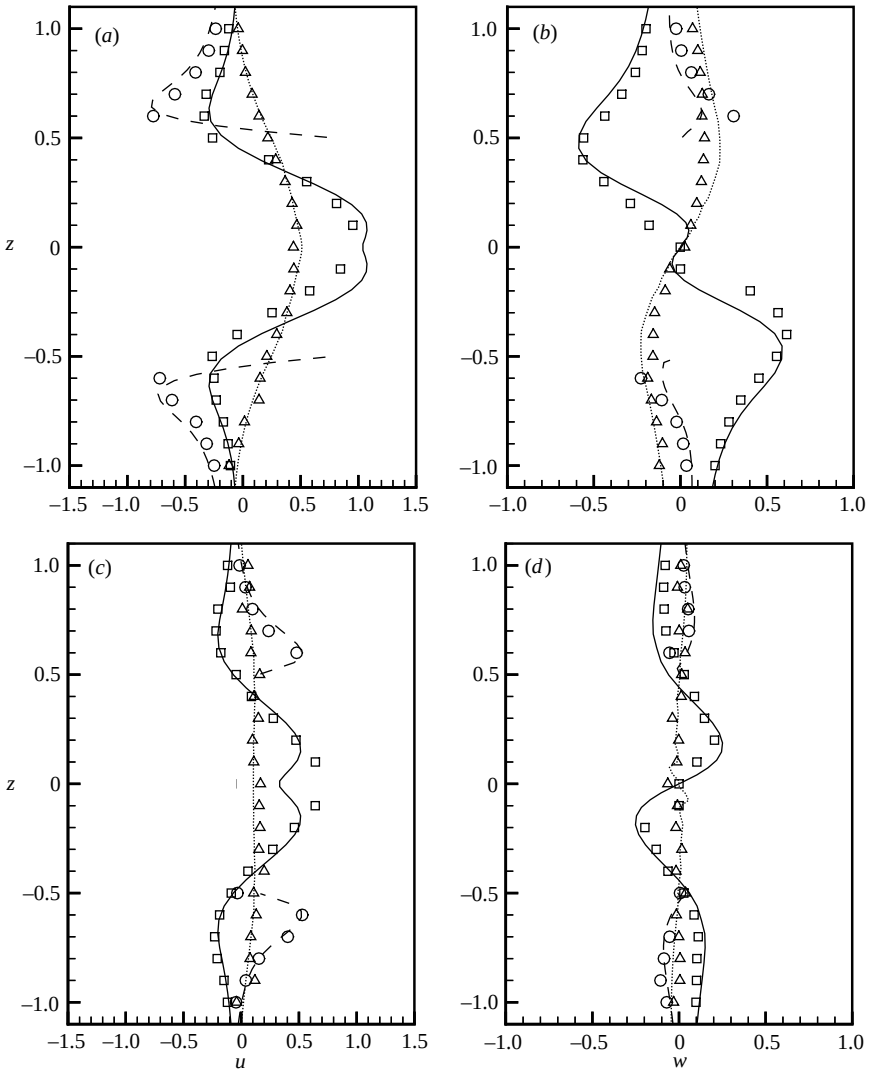

FIGURE 4. Comparison between the velocity components obtained with the three-dimensional model and those measured in the experiments by Dutsch *et al.* (1998), at three transversal sections in regime A, $KC = 5$, $\beta = 20$, $Re = 100$: (*a*) streamwise component at $t_p = 0.75$; (*b*) transversal component at $t_p = 0.75$; (*c*) streamwise component at $t_p = 1.0$; (*d*) transversal component at $t_p = 1.0$. Symbols and lines refer respectively to experimental and numerical data (△, $x = -0.8$; ○, $x = 0$; □, $x = 0.8$.)

3. Regime D: results

Regime D of TB90 is characterized by an asymmetric vortex shedding in the (x, z)-planes and by three-dimensional motion. The asymmetric vortex shedding gives rise to a periodic transversal force, whose period is half that of the imposed oscillation.

In their visual analysis, TB90 have observed that vorticity is shed obliquely from one side to the other one with respect to the plane $z = 0$, across the axis of oscillation (a detailed description of this regime is given in TB90). The flow visualization by TB90 has also shown the presence of well-defined three-dimensional vortex structures whose length is a function of β and KC. For $\beta = 20$ and $KC = 6.5$ the average,

L_x/D	L_y/D	L_z/D	$n_x \times n_y \times n_z$	n_{cir}	$F_{x,rms}$	$F_{z,rms}$
26	12	14	$72 \times 48 \times 88$	48	2.76	0.59
26	–	14	$72 \times 0 \times 88$	48	2.74	0.66

TABLE 2. Parameters of the simulations and r.m.s. values of the longitudinal and transversal forces for the cases studied in regime D ($KC = 6.5$, $\beta = 20$). n_{cir} denotes the number of grid points placed along the circumference of the cylinder. The vertical grid spacing is $\Delta y = D/4$. The two-dimensional simulation was carried out using a two-dimensional version of the present three-dimensional model.

non-dimensional axial wavelength λ has been observed to be roughly equal to 4. We carried out computations considering an axial length of 12 diameters that allowed small-scale three-dimensional modes (according to the definition given by YR02) to develop. We have also performed computations using a two-dimensional version of the solver in order to compare the results obtained with a two-dimensional model against those of the three-dimensional simulations. The cases investigated for regime D together with the computational parameters are reported in table 2. The simulations were carried out for 160 cycles.

During the first few cycles of oscillation the flow field developed symmetrically and vortex shedding was similar to that of regime A (not shown here). Later on, the flow field became unstable in that a vortex shed from one side grew larger than that on the opposite side with respect to the plane $z = 0$. This produced the progressive rise in the asymmetric vortex shedding that eventually leads to the V-pattern clearly shown in TB90.

Our computations showed that, unlike the experiments by TB90, the V-pattern is not stable; rather we observed that the flow convected to one side of the $z = 0$ plane intermittently changed its direction to the other side. The period of this switching was much larger (typically 20 to 50 times) than the period of oscillation of the fluid. This intermittent switching has already been observed in the experiments by TB90, but for regime E only. Specifically, they found that both regimes (D and E) exhibit the V-shaped two-dimensional vortex pattern, the only difference being in the stable V-pattern appearing in regime D and in the intermittent switching characterizing regime E. By contrast, our results show that this switching also occurs in regime D. In order to confirm that this result was not an artifact of the numerical scheme or of the boundary conditions employed, we ran a 230-cycle simulation with the two-dimensional (ω–ψ) code of Pentek *et al.* (1998) using 128×128 grid points respectively in the circumferential and in the radial directions. The results of the two-dimensional simulation (not reported here) showed that the first switching from a V-pattern to its mirror-image occurred after about 100 cycles, and it repeated at irregular intervals during the rest of the simulation. Hence, regime D appears to be an asymmetric regime characterized by vortex shedding in a V-pattern that is intermittently switched in time from one side to the other one with respect to the axis of oscillation. Switching from a V-pattern to its mirror-image seems to be related to a two-dimensional instability of the flow field, since it can be reproduced using a two-dimensional simulation. It is not easy to explain why this intermittent switching occurs. TB90 attributed it to the presence of small disturbances in the flow field. Dutsch *et al.* (1998) have performed a stability investigation of a flow regime characterized by the presence of two modes (one and its mirror-image) finding that the asymmetric cyclic vortex pattern was only weakly stable and that deviations from

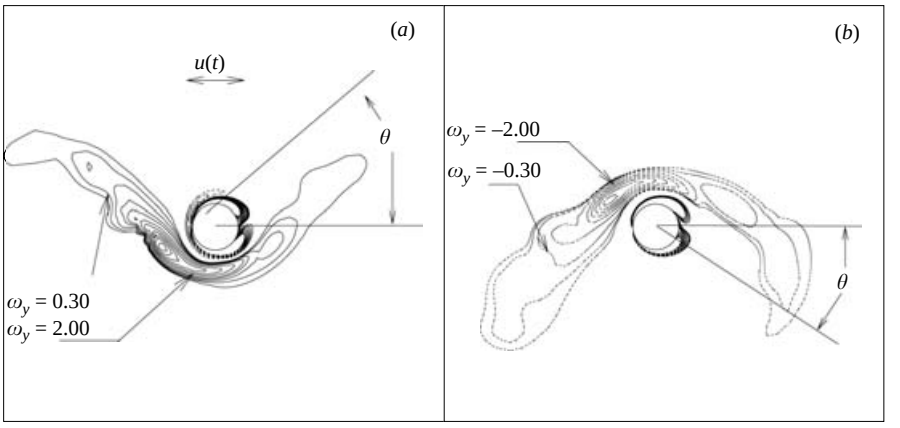

FIGURE 5. Iso-lines of the vorticity component ω_y: (*a*) positive vorticity of the upward V-pattern at the 96th cycle; (*b*) negative vorticity of the downward V-pattern at the 130th cycle. Regime D, $KC = 6.5$ and $\beta = 20$, $Re = 130$. θ denotes the angle of inclination of vortex shedding with respect to the longitudinal axis. Note that ω_y drops by almost one order of magnitude within three diameters from the cylinder.

periodicity could be detected during the simulation. On the basis of Dutsch *et al.* (1998), TB90 and our results, it might be argued that, since a mode of oscillation is weakly stable, the presence of small disturbances, which are always present either in a laboratory experiment or in a numerical one, may trigger the transition from one mode to its mirror-image.

Figure 5 shows the iso-lines of the axial component of vorticity ω_y at $y = 0$ at two different cycles during the oscillation, namely the 96th and the 130th cycles. The visualizations of figure 5 clearly show the presence of the two mirror-image modes during the oscillation, namely the upward and the downward V-shaped vortex patterns. Each V-pattern is associated with alternate positive and negative vorticity shed obliquely every half-cycle depending on the sign of the large vortex generated on the opposite side. Our results are consistent with both the visualization of TB90 (see for example their figures 18 and 19) and with the numerical results for regime E shown in figure 21 of Dutsch *et al.* (1998).

The time evolution of the V-patterns has its counterpart in the time record of the forces acting over the cylinder. Our results show that switching from one V-pattern to its mirror-image gives rise to a bump-like behaviour in the time record of the longitudinal force F_x (figure 6*a*i) and to severe modulations of the transversal force F_z (figure 6*b*i), with a time scale order 50 cycles. This behaviour is related to the direction of vortex shedding and, specifically, to the angle θ defined in figure 5. By definition, θ is equal to 0 when the V-pattern degenerates into a straight line and vorticity is shed symmetrically along the longitudinal direction, as in regime A. When $\theta = 0$ (for example along the first 15 cycles of the simulation) the maximum value of the force F_x remains nearly unchanged from cycle to cycle, whereas the transversal force F_z is absent. Later, the asymmetry causes vorticity to be shed in the V-pattern, producing a reduction in the maximum of F_x over a cycle and an increase in the maximum of F_z. Note that an increase in the maximum longitudinal force is associated with a decrease in the maximum transversal force and vice versa. When θ is large, vortex shedding is strongly asymmetric, the maximum of F_z is large and that of F_x decreases; conversely, when θ is small, vortex shedding tends to be

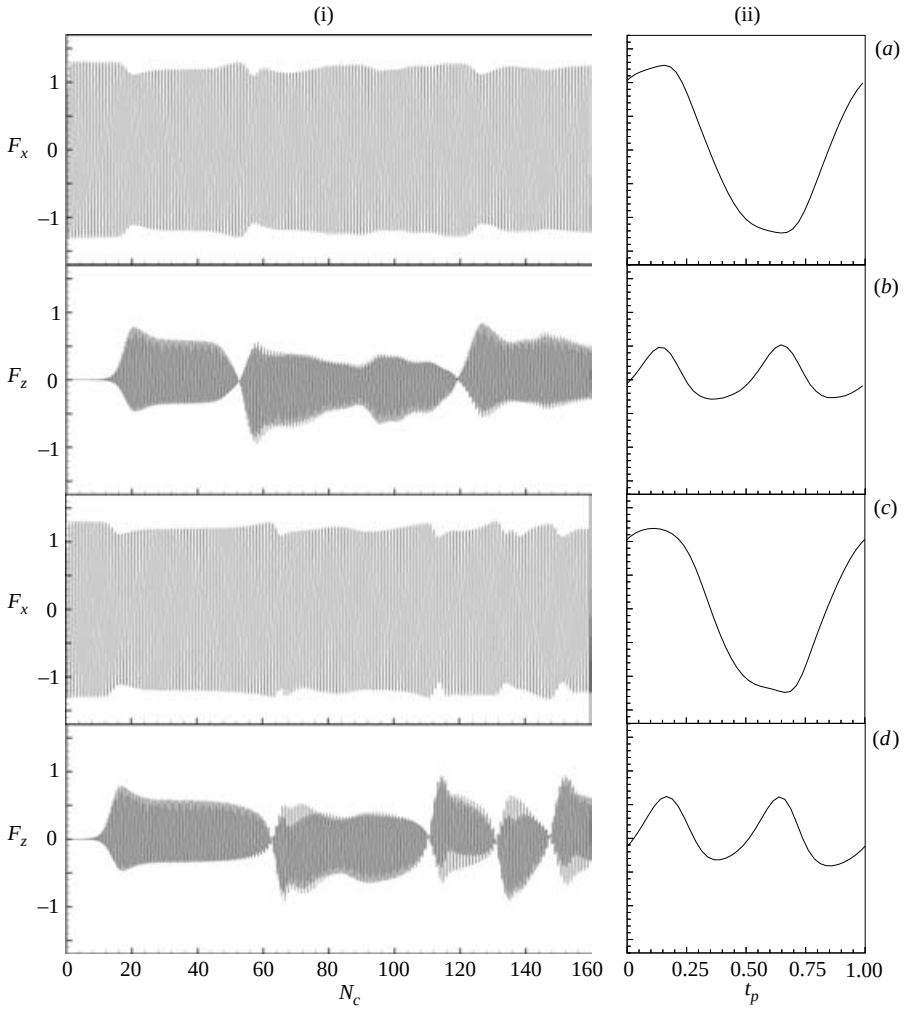

FIGURE 6. Evolution of the in-line (F_x) and transverse (F_z) components of the force along the cycles, obtained in the three-dimensional and two-dimensional simulations. Also shown are the time evolution of the forces during a cycle: (*a*i) longitudinal force of the three-dimensional simulation; (*a*ii) longitudinal force of the three-dimensional simulation during the 159th cycle; (*b*i) transversal force of the three-dimensional simulation; (*b*ii) transversal force of the three-dimensional simulation during the 159th cycle; (*c*i) longitudinal force of the two-dimensional simulation; (*c*ii) longitudinal force of the two-dimensional simulation during the 137th cycle; (*d*i) transversal force of the two-dimensional simulation; (*d*ii) transversal force of the two-dimensional simulation during the 137th cycle. Regime D, $KC = 6.5$, $\beta = 20$, $Re = 130$.

more symmetric with respect to the $z = 0$ plane, the maximum of the longitudinal force increases and that of F_z decreases. When a V-pattern turns into its mirror-image ($N_c \sim 52$, $N_c \sim 120$), the maximum along the cycle of F_x increases while the transversal force tends to disappear. This is due to the symmetry recovered in the vorticity field, in that, for few cycles, the V-pattern degenerates into a straight line ($\theta \sim 0$).

In order to check how three-dimensional motion affects the dynamics of vortex shedding we compared the three-dimensional results with those obtained with a

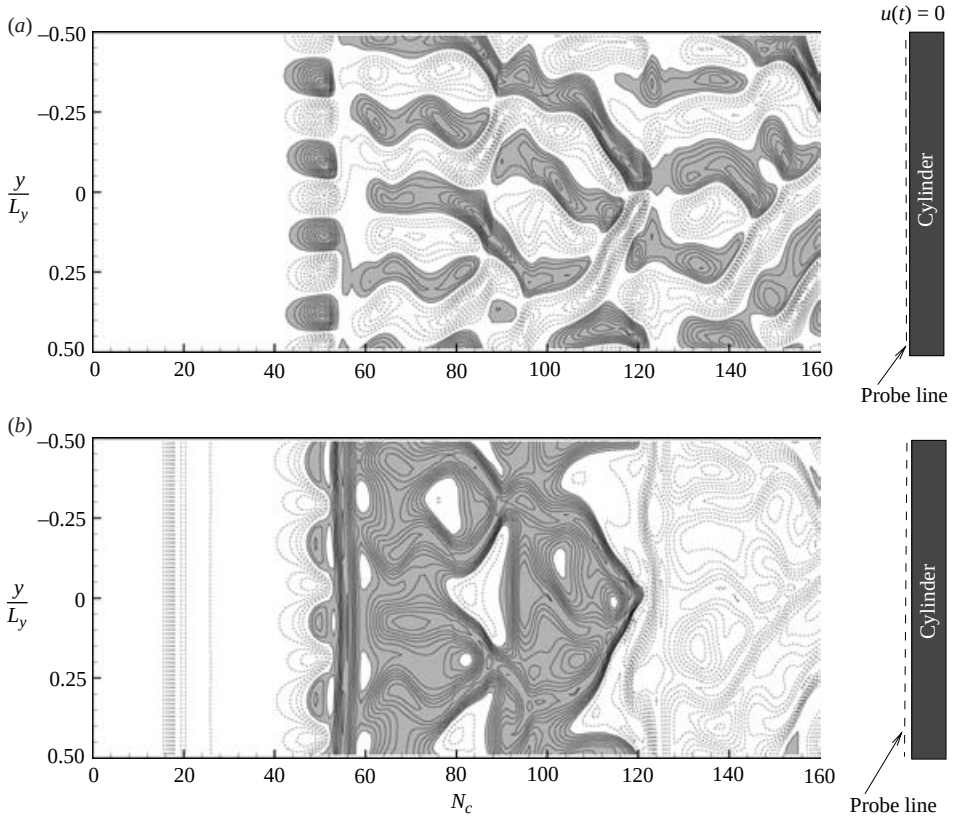

FIGURE 7. Space–time evolution of the non-dimensional vorticity components along the probe line $x = -0.503$, $z = 0$, at the phase $t_p = 0$. (*a*) ω_z; (*b*) ω_y. Grey and white areas denote respectively positive and negative vorticity. Regime D, $KC = 6.5$, $\beta = 20$, $Re = 130$.

two-dimensional simulation using the same grid and boundary conditions in the (x, z)-plane as in the three-dimensional case (see table 2).

Figure 6 shows that three-dimensionality in the flow tends to stabilize the presence of a V-pattern, in that it increases the time scale for the occurrence of switching from a mode to its mirror-image.

Three-dimensional vortex patterns appeared during the simulation after the occurrence of the two-dimensional instability generating the V-patterns. Figure 7 shows the evolution in time of the vorticity components ω_z and ω_y along the line of the symmetry plane ($z = 0$) at the first grid point off the surface of the cylinder $x = -0.503$, and at a phase $t_p = 0$ corresponding to zero outer velocity. The analysis of figure 7 and figure 8 shows that an axial mode (A_4) with wavelength $\lambda = 3$ appears first. Triggering of three-dimensionality occurs around the 30th cycle, well beyond the cycle at which the two-dimensional asymmetric motion that generates the V-shaped vortex shedding appears. The amplitude of the three-dimensional mode rapidly increases leading to regular vortex structures as clearly seen in figure 7. Such three-dimensional vortex structures persist up to about the 52nd cycle of oscillation. It is remarkable that a two-dimensional, asymmetric, downward V-pattern (similar to that of figure 5*b*) starts to develop around the 10th cycle and maintains its direction up to the 52nd cycle. At this cycle, a switching occurs from the downward V-pattern to its mirror-image;

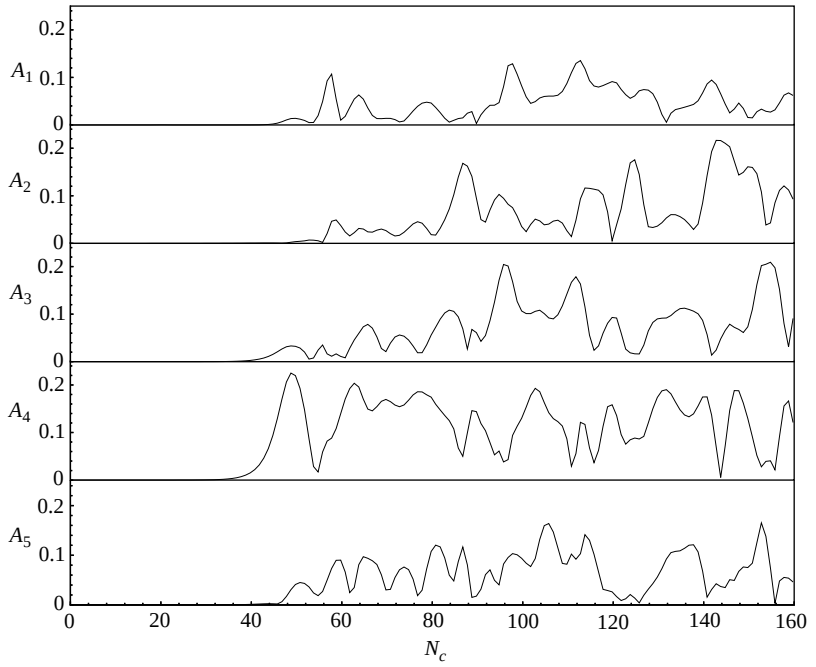

FIGURE 8. Time evolution of the amplitude of the relevant Fourier modes of the vorticity components ω_z of figure 7(a). A_i denotes the amplitude of the mode with wavelength L_y/i. Regime D, $KC = 6.5$, $\beta = 20$, $Re = 130$.

the amplitude of the $\lambda = 3$ mode decays and a mode with wavelength $\lambda = 1$ forms. Thereafter, an upward V-pattern (as in figure 5a) develops, causing the change of sign in the transversal vorticity ω_z that, in the space–time plot of figure 7(a), exhibits a sort of chess-board pattern. The three-dimensional motion now appears less regular and the Fourier analysis of the vorticity shows the presence of five axial modes. Another switching from the positive to the negative V-pattern occurs around the 120th cycle, and, like the one occurring around the 52nd cycle, it is accompanied by significant three-dimensional activity. The spatial distribution of the vorticity components ω_z and ω_y at $t_p = 0$ in the plane $z = 0$ at three significant cycles (figure 9) reflects the results of the above Fourier analysis. Specifically, a single dominant wavelength was not discernible during the simulation; rather, visual analysis of the vorticity field (figure 9) shows that the dominant wavelength changes during the simulation. It is worth noting that the vortex patterns shown in figure 9(b) are qualitatively in very good agreement with the dye pattern in figure 20 of TB90.

The visual analysis suggests that, on average, vortex structures with wavelengths ranging between 3 and 6 are observed in the present case, although λ intermittently changes during the simulation. However, it should be pointed out that, although the visual analysis allows identification of a fundamental axial mode, the Fourier analysis shows that five different modes contribute to the axial distribution of the vorticity field, and three of them, namely the 2nd, 3rd and 4th, appear to dominate the others.

The main component of vorticity, ω_y, does not maintain its sign along the probe line of figure 7. This behaviour corresponds to the presence of the sinuous S-mode already detected in the experimental investigation by YR02. Like that study, we found that the occurrence of the sinuous S-mode is intermittent in time, in that it

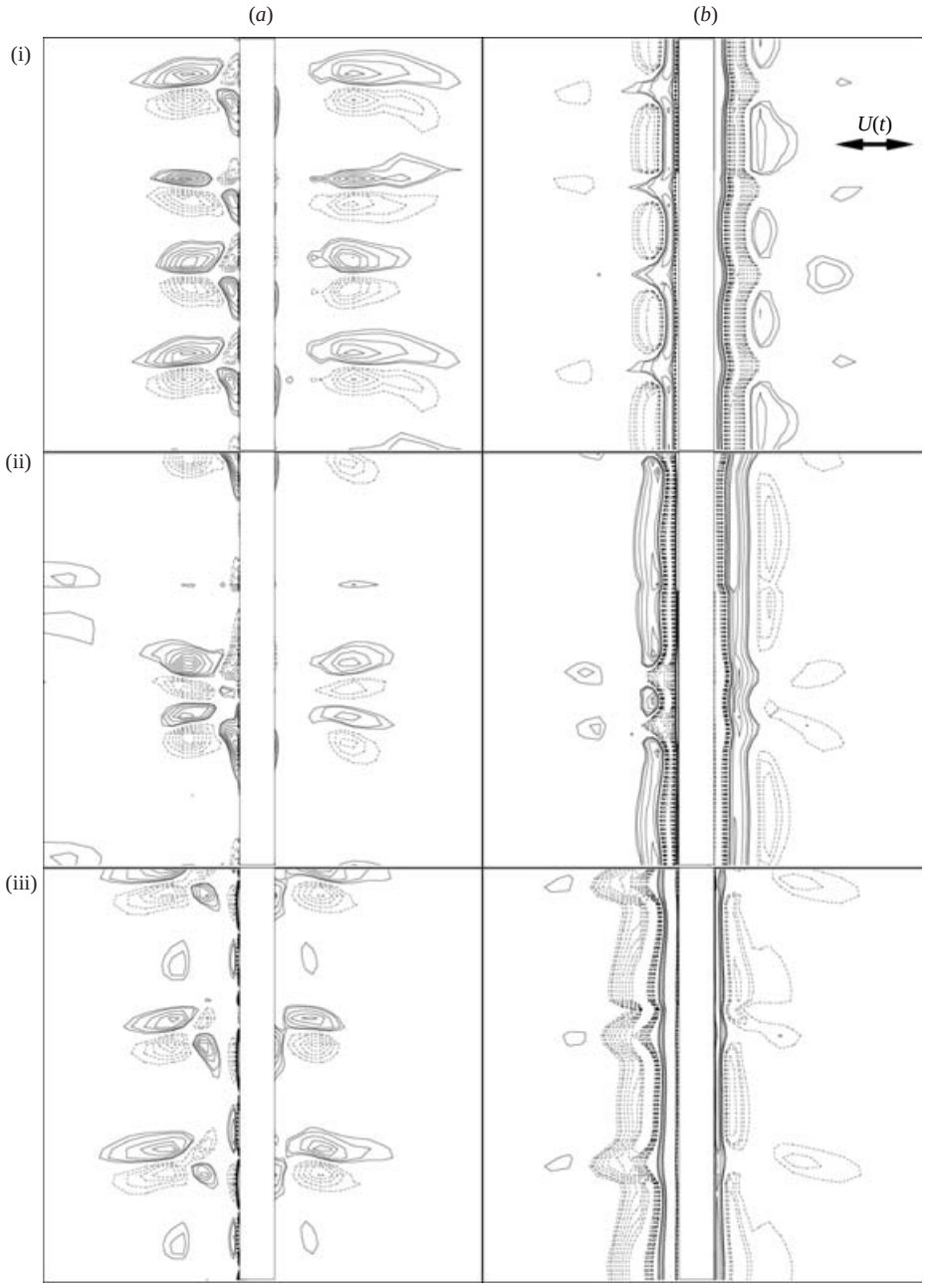

FIGURE 9. Iso-lines of vorticity components in the plane $z = 0$ at $t_p = 0.25$: (*a*) ω_z and (*b*) ω_y at (i) $N_c = 64$, (ii) $N_c = 144$ and (iii) $N_c = 160$. Regime D, $KC = 6.5$, $\beta = 20$, $Re = 130$.

can be detected only in small time windows, whereas for most cycles during the simulation the presence of the three-dimensional unidirectional U-mode is observed. This phenomenon can be explained through detailed analysis of the vorticity field. Specifically, the occurrence of the S-mode is not necessarily associated with the simultaneous presence of the two V-patterns along the axial direction (one and its mirror-image), or with the occurrence of a complete switching from a two-dimensional

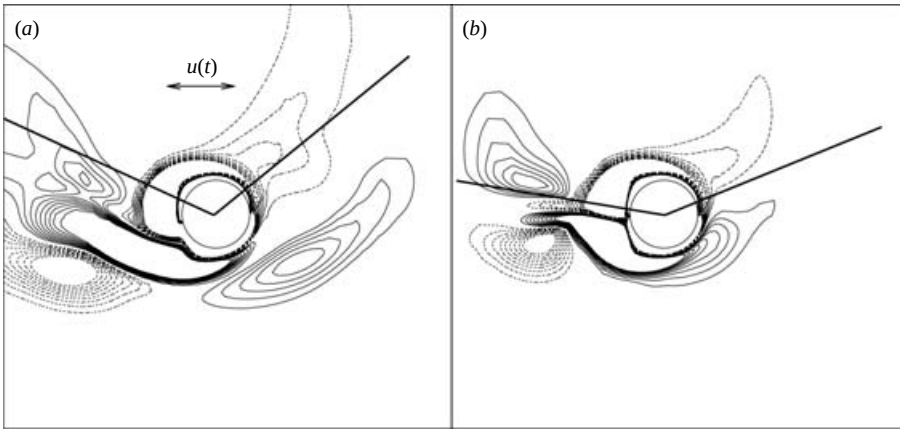

FIGURE 10. Iso-lines of the vorticity component ω_y at $t_p = 0$ of the 112nd cycle at two different axial sections: (*a*) $y_d/L_y = -0.06$; (*b*) $y_d/L_y = -0.26$. Regime D, $KC = 6.5$, $\beta = 20$, $Re = 130$. The straight lines indicate the degree of opening of the V-pattern.

mode to its mirror-image along y. In particular, figure 7(*b*) shows that the S-mode occurs around the 52nd and the 120th cycles, which are characterized by complete switching of the two-dimensional mode, and around the 80th cycle, where complete switching is not observed. In our computations the presence of the S-mode appears to have been caused by two main factors: circumferential motion of the main two-dimensional mode (a V-pattern) along y accompanied by a variation of the angle of opening of the V-pattern along y; and the fact that complete switching from a V-pattern to its mirror-image does not occur at the same time along y but appears delayed in time from section to section. The circumferential effect (rotation of the V-pattern from section to section along y) and the variation of the degree of opening of the V-pattern along y are clearly seen in figure 10, which shows the iso-lines of ω_y at two significant x, z sections, $y_d/L_y = -0.06$ and $y_d/L_y = -0.26$. The above-mentioned effects produce a variation in the angle of inclination θ of vortex shedding along y. Figure 10 shows the 112nd cycle, well before the occurrence of complete switching from one V-pattern to the other one.

The occurrence of the three-dimensional described above effects influences the axial distribution of the sectional load as well as the axial integrated values.

Figure 11 shows the maximum variation of the non-dimensional sectional forces, compared to the corresponding axial-integrated values F_x and F_z. The maximum variation $\Delta F_x = F^s_{x,max} - F^s_{x,min}$ of the longitudinal sectional force is small (figure 11*a*); indeed it does not exceed 10% of F_x. This result corroborates and extends the finding by YR02. By indirect analysis of the experimental data, YR02 found that the effect of the S-mode on the axial variation of the longitudinal force is small.

On the other hand, three-dimensional motion appears to dramatically affect the axial distribution of the transversal force. Figure 11(*b*) shows that after the three-dimensional flow field has fully developed, significant variations of the sectional force are recorded along y. On average $\Delta F_z = F^s_{z,max} - F^s_{z,min}$ amounts to about $50-60\%$ of F_z, although, sometimes, values of ΔF_z even larger than F_z are recorded. We found that large three-dimensional effects in the transversal force appear in conjunction with the occurrence of the three-dimensional S-mode. In particular, the increase of three-dimensionality, quantified by ΔF_z, is associated with a general reduction in the

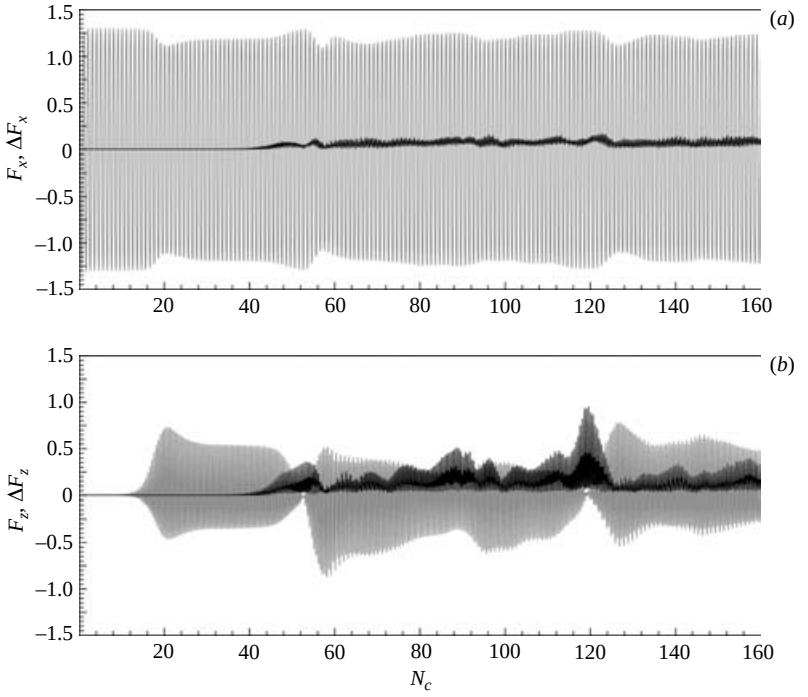

FIGURE 11. Time-record of the force components (grey line) and of the maximum variation of the sectional forces $\Delta F_i(t)$ (black line): (*a*) longitudinal components; (*b*) transversal components. Regime D, $KC = 6.5$, $\beta = 20$, $Re = 130$.

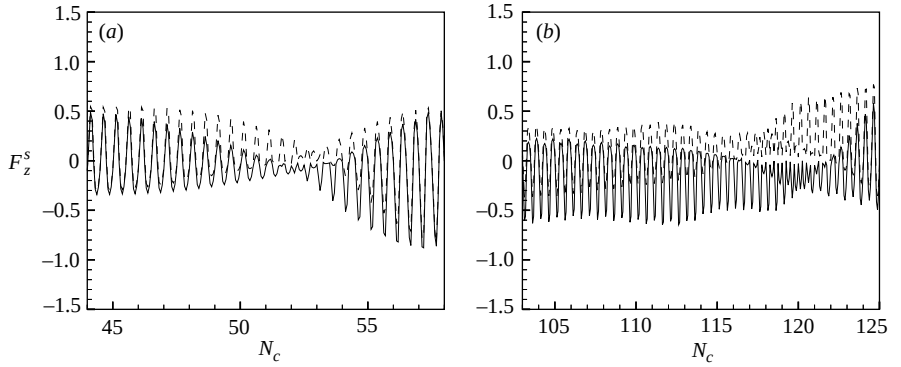

FIGURE 12. Time evolution of the maximum (- - -) and minimum (—) values of the sectional transversal force F_z^s: (*a*) around the 52nd cycle; (*b*) around the 120th cycle. Regime D, $KC = 6.5$, $\beta = 20$, $Re = 120$.

axial integrated value F_z. It is remarkable that ΔF_z is large when switching from a V-pattern to its mirror-image occurs, and, interestingly, very large values of ΔF_z are recorded when the axial-integrated value F_z is roughly 0. This behaviour can be explained by looking at figure 12, which reports the time record of the maximum and minimum values of the sectional force around the first switching ($44 < N_c < 58$) and the second one ($103 < N_c < 125$). Analysis of figures 7(*b*), 11, 12 suggests that

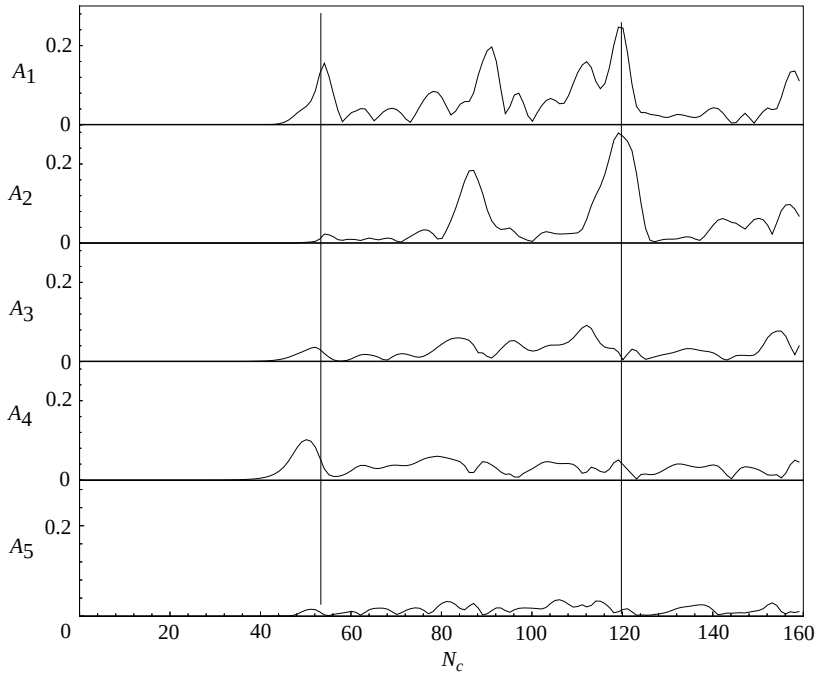

FIGURE 13. Time evolution of the amplitude of the relevant Fourier modes of the transversal sectional force $F_z^s(y)$ at $t_p = 0.125$. A_i denotes the amplitude of the mode with wavelength L_y/i. The vertical lines indicate the cycles at which complete switching from a V-pattern to its mirror-image occurs. Regime D, $KC = 6.5$, $\beta = 20$, $Re = 130$.

when a V-pattern is well developed and repeats without appreciable variations of θ along the axial direction, the unidirectional U-shaped mode is observable along y and the axial variation of the sectional transversal force is always smaller than the axial-integrated value F_z. This is due to the fact that the sectional force maintains its sign along the axis. On the other hand, when large variations of θ occur, giving rise to the S-mode, the sectional transversal force changes its sign along the axis, and the axial integrated value is smaller than the maximum variation of the sectional force. By way of example, inspection of figure 12 shows that, on approaching the cycle at which complete switching occurs along y, the difference between the maximum and the minimum values of the sectional force progressively increases but still maintains its sign; later, in the region of the switching, $F^s_{z,max}$ and $F^s_{z,min}$ have opposite signs; finally, after that switching has been completed and the new V-pattern repeats along y with small variations in θ the sectional force again maintains its sign during the oscillation.

The Fourier analysis of the transversal sectional force at $t_p = 0.125$, at which the axial integrated value is close to the maximum, shows that the large variation in the sectional force along the axis is related to the presence of the 1st as well the 2nd mode, which appear to be dominant when the S-mode is present (figure 13). Finally, figure 14 shows a three-dimensional view of the time evolution in the 120th cycle of the distribution of the sectional transversal force along the axial direction. This clearly shows that the transversal force does not maintain its sign along the axial direction and that the large-scale modes mostly contribute to the large variation in the sectional force.

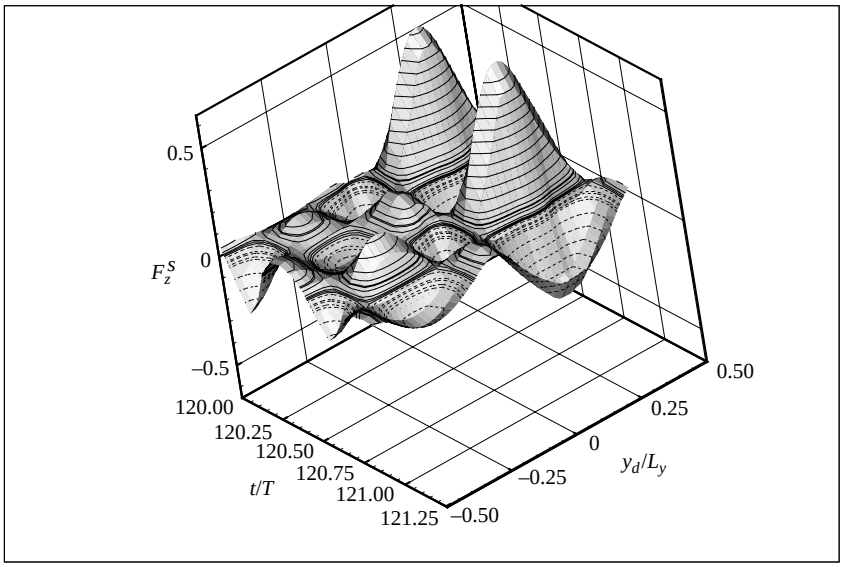

FIGURE 14. Evolution during the 120th cycle of the axial distribution of the sectional transversal force $F_z(y_d/L_y, t/T)$. Regime D, $KC = 6.5$, $\beta = 20$, $Re = 130$. For the coordinate system see figure 2.

4. Regime F: results

Regime F is a double-pair diagonal regime, in which vorticity is shed diagonally with respect to the axis of oscillation. The mechanism of vortex shedding has been described by several authors (see for example Williamson 1985; TB90; Dutsch *et al.* 1998) and will not be repeated here. The angle of inclination of the diagonal pattern with respect to the longitudinal axis increases with KC. The results of the visual analysis of TB90 show that for $KC < 10$ the angle of inclination of the diagonal vortex pattern θ is small, and, in the far field, the pattern tends to be parallel to the longitudinal axis. As KC increases ($KC > 10$) the angle of inclination of the pattern increases, and vorticity is convected along a straight line that, in the far field, maintains its angle of inclination. Since there is no reason for vortex shedding to stay along one diagonal rather than the other during the oscillation, intermittent switching may occur during the oscillation, similar to that observed in regime D.

Three-dimensional structures have been observed during the oscillation in the laboratory experiments of both TB90 and Dutsch *et al.* (1998). These structures have been shown to repeat periodically over an axial wavelength within the range $3.5 < \lambda < 6$ for β ranging between 10 and 40. The wavelength λ also depends on the KC parameter, although, as stressed in TB90, *any dependence of* λ *on* KC *remains obscure*. For the case examined in our investigation $KC = 8.5$, $\beta = 20$, the axial length of the cylinder chosen was equal to 12 diameters, which allowed for small-scale axial modes to develop. As in Regime D, we also ran an equivalent two-dimensional simulation (table 3). The simulations were carried out for 160 cycles.

Figure 15 shows the axial vorticity ω_y at four different phase positions in the half-cycle, after the asymmetric diagonal vortex shedding has developed. The shape of the diagonal pattern, well shown for example in figure 15(b, c), is consistent with the value of the Keulegan–Carpenter number ($KC < 10$), and is similar to that of figure 25 of TB90. The resulting vortex shedding gives rise to longitudinal as well as

L_x	L_y	L_z	$n_x \times n_y \times n_z$	n_{cir}	$F_{x,rms}$	$F_{z,rms}$
26	12	14	$128 \times 72 \times 104$	64	2.13	0.61
26	—	14	$128 \times 0 \times 104$	64	2.11	0.76

TABLE 3. Parameters of the simulations, and r.m.s. values of the force components for the case studied in regime F ($KC = 8.5$, $\beta = 20$, $Re = 170$). The axial grid spacing is $\Delta y = D/6$. The two-dimensional simulation has been carried out using a two-dimensional version of the present three-dimensional model.

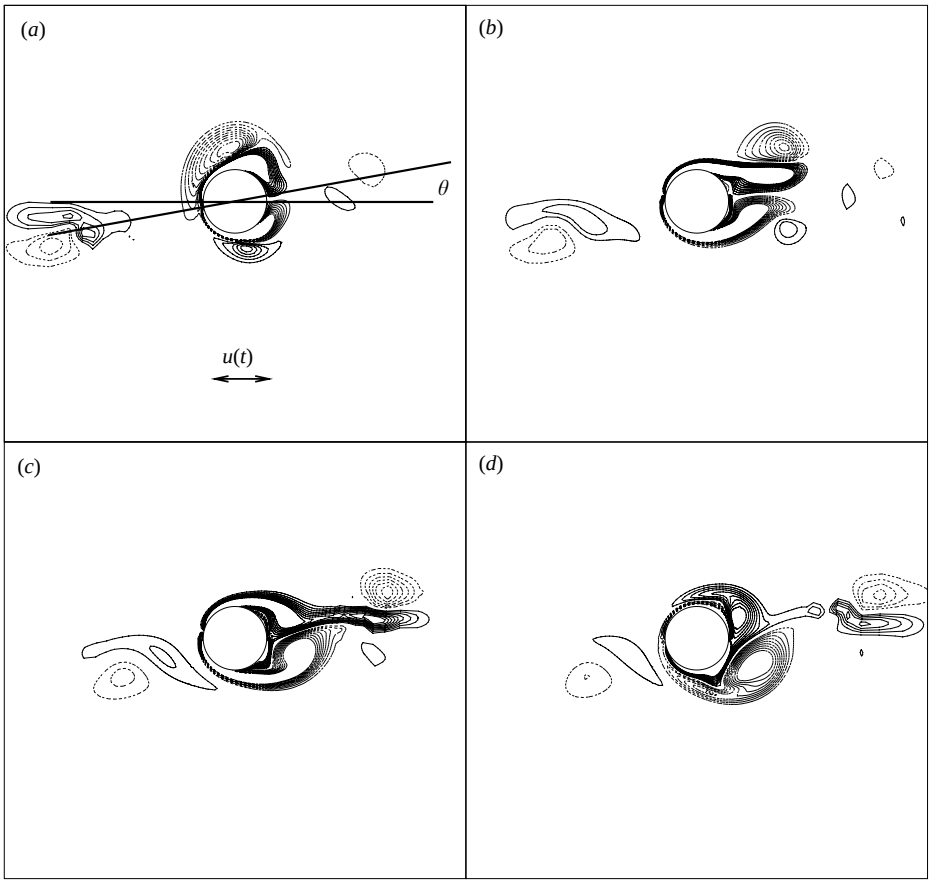

FIGURE 15. Iso-lines of the vorticity component ω_y in the plane $y = 0$ after the diagonal pattern has developed ($N_c = 42$): (*a*) $t_p = 0.125$; (*b*) $t_p = 0.250$; (*c*) $t_p = 0.375$; (*d*) $t_p = 0.500$. Regime F, $KC = 8.5$, $\beta = 20$, $Re = 170$. The angle θ between the straight lines roughly indicates the inclination of the diagonal pattern with respect to the longitudinal axis.

transversal forces, as shown in figure 16. During the first few cycles the flow field is symmetric with respect to the plane $z = 0$, the time record of F_x appears regular and repeats without appreciable differences from cycle to cycle, and the transversal force is absent. Thereafter, the instability leading to the diagonal vortex shedding increases and a significant transversal force is recorded. It is worth noting that, unlike regime D, the increase in the diagonal vortex shedding does not significantly affect the longitudinal force. This is because the inclination of the diagonal pattern with

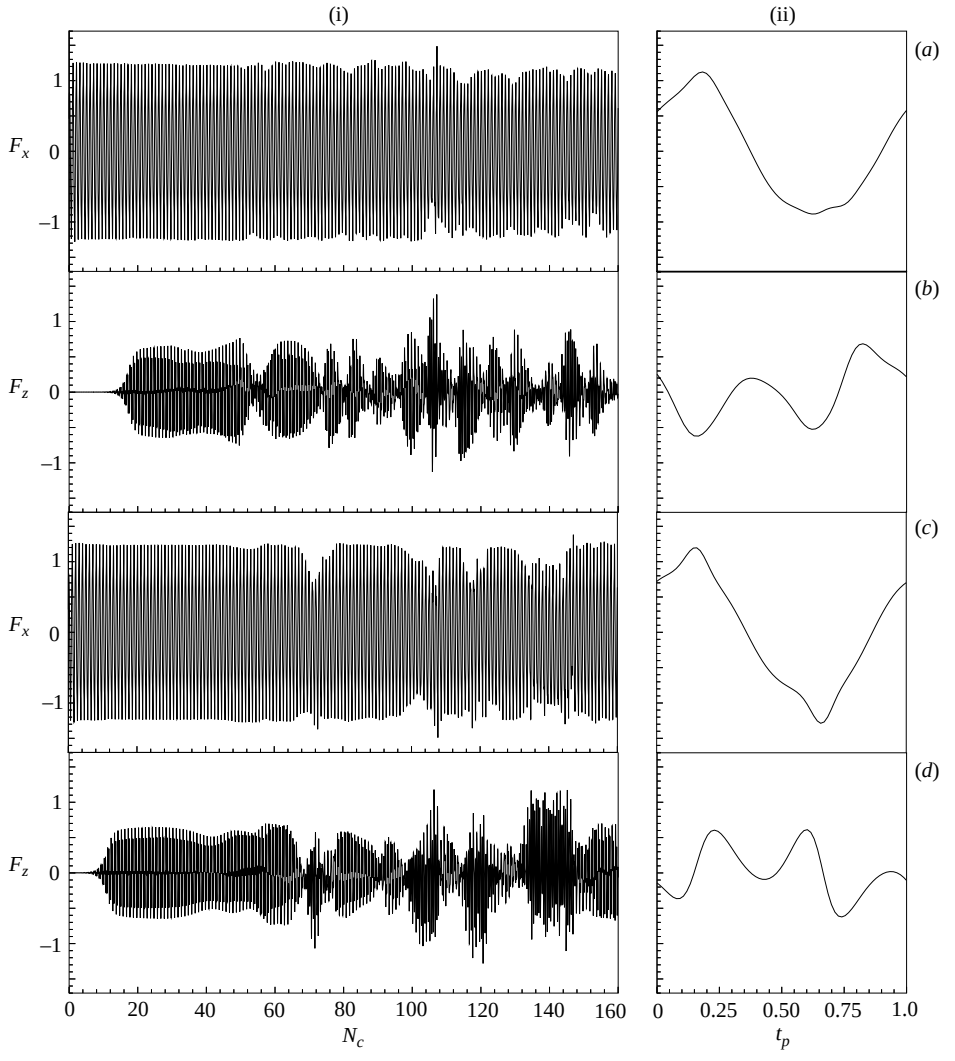

FIGURE 16. Time evolution of the in-line (F_x) and transverse (F_z) components of the force obtained in the three-dimensional and two-dimensional simulations: Also shown are the typical time evolution of the forces during a cycle: (*a*i) longitudinal force of the three-dimensional simulation; (*a*ii) longitudinal force of the three-dimensional simulation during the 153rd cycle; (*b*i) transversal force of the three-dimensional simulation; (*b*ii) transversal force of the three-dimensional simulation during the 153rd cycle; (*c*i) longitudinal force of the two-dimensional simulation; (*c*ii) longitudinal force of the two-dimensional simulation during the 153rd cycle; (*d*i) transversal force of the two-dimensional simulation; (*d*ii) transversal force of the two-dimensional simulation during the 153rd cycle. Regime F, $KC = 8.5$, $\beta = 20$, $Re = 170$.

respect to the plane $z = 0$ is small. After approximately 30 more cycles the diagonal pattern has developed, the first switching from this pattern to its mirror-image occurs, and it repeats at irregular intervals during the simulation. Interestingly, the time scale of switching is much smaller (order 6 cycles) than that observed in regime D. Furthermore, comparison between figure 16(*b*i) and figure 16(*d*i) shows that three-dimensionality in the flow field seems to enhance the occurrence of switching, as

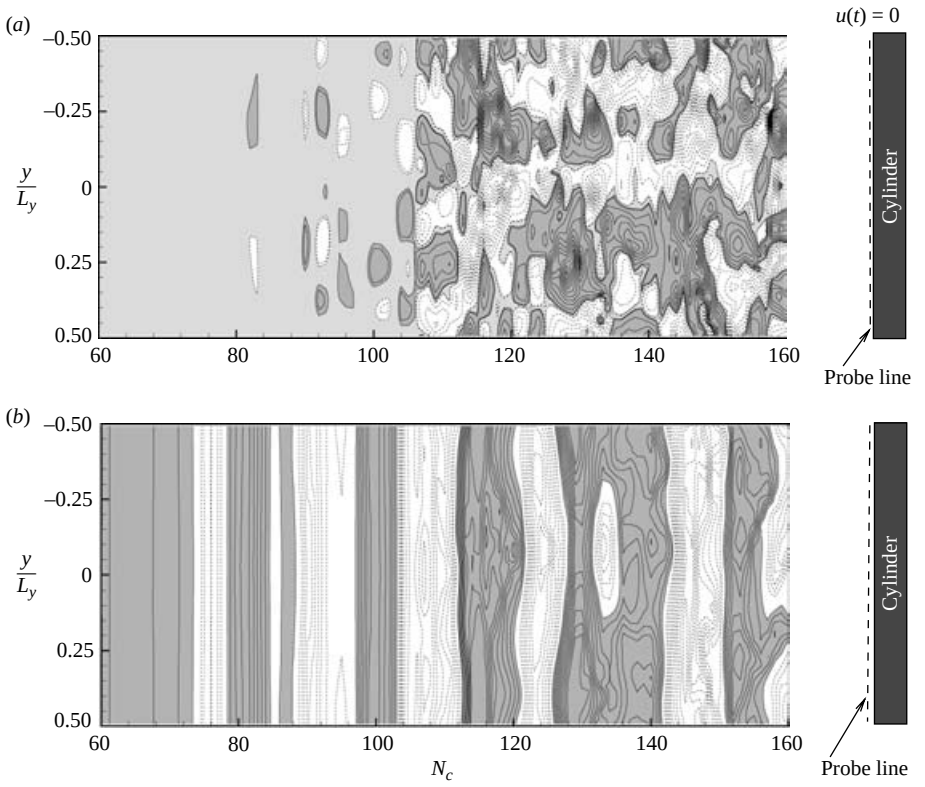

FIGURE 17. Space–time evolution of the non-dimensional vorticity components along the probe line $x = -0.502$, $z = 0$, at the phase $t_p = 0$. (*a*) ω_z; (*b*) ω_y. Grey and white areas denote respectively positive and negative vorticity. Regime F, $KC = 8.5$, $\beta = 20$, $Re = 170$.

seen when comparison is made with an equivalent two-dimensional case. Switching from a diagonal pattern to its mirror-image produces a bump-like behaviour of the longitudinal force and severe modulations of the transversal one.

The time evolution of the vorticity components ω_z and ω_y along the probe line $z = 0$, $x = -0.502$ shown in figure 17 shows negligible three-dimensional activity during the first 60 cycles. As in regime D, three-dimensional modulation of the vorticity field occurs well beyond the cycles at which asymmetry with respect to the plane $z = 0$ takes place. Moreover, switching from one two-dimensional mode to its mirror-image can be reproduced by pure two-dimensional simulations, thus showing that the dynamics of vortex shedding in the cross-sectional plane is not related to three-dimensionality in the flow field. The time evolution of the amplitudes of the relevant Fourier modes of the vorticity ω_z (figure 18) shows that the first mode A_1 with wavelength $\lambda = 12$ first develops, and that thereafter additional small-scale modes, with wavelength ranging from 6 to 2.4, appear. Unlike regime D, the leading modes are now the 1st, 2nd and 3rd. As in regime D, visual analysis of the vorticity component ω_y (not reported here) shows three-dimensional vortex structures in qualitative agreement with the dye pattern visualized in figure 27 of TB90.

Interestingly, an increase in KC, with a constant value of β, produces an increase in the average wavelength of the three-dimensional vortex structures along the axial direction, compared to the previous case of regime D. This phenomenon has already been observed by YR02, although in their analysis it was not clear whether this effect

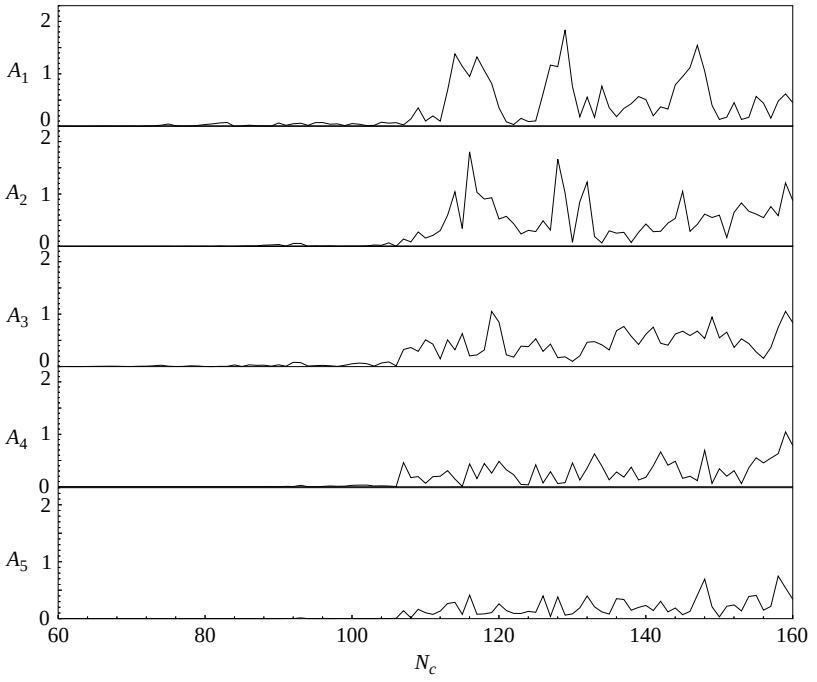

FIGURE 18. Time evolution of the amplitude of the relevant Fourier modes of the vorticity components ω_z of figure 17(a). A_i denotes the amplitude of the mode with wavelength L_y/i.

could be ascribed to the increase in KC or to the increased three-dimensionality of the external flow field. In the experiments by YR02, the increase in KC was strictly related to a corresponding increase of the orbital motion of the fluid particles and consequently to the increased three-dimensionality of the external motion. Our analysis, carried out in a unidirectional flow field, shows that the increase of KC by itself causes the increase in the dominant axial wavelength.

Analysis of figure 17 suggests that, after the three-dimensional motion has fully developed, the sinuous S-mode appears along the axial direction, at irregular intervals which are not entirely correlated to the occurrence of switching from a two-dimensional diagonal pattern to its mirror-image. As in regime D, the sinuous S-mode seems to be related to the circumferential motion undergone by the main sectional vortex structure (diagonal pattern) along the axial direction. Of course, the simultaneous presence of the two two-dimensional modes (one and its mirror-image) along the axis of the cylinder, already detected in the experimental analysis by Obasaju *et al.* (1988) and by YR02 is a prime cause of the sinuous S-mode developing. Nevertheless, in the present investigation, in which this phenomenon does not occur, we find that the circumferential rotation of the main two-dimensional structure contributes to the generation of the sinuous axial S-mode.

Figure 19 shows the maximum variation in the sectional forces in time compared to the corresponding axial-integrated values. As in the previous case (regime D), the maximum variation in the transversal force is much larger than that of the longitudinal one. Specifically, on average, ΔF_x is about 20% of the axial-integrated value, whereas ΔF_z is always larger than the corresponding axial integrated value F_z. Furthermore, the maximum variation in the sectional forces, as a percentage of the corresponding

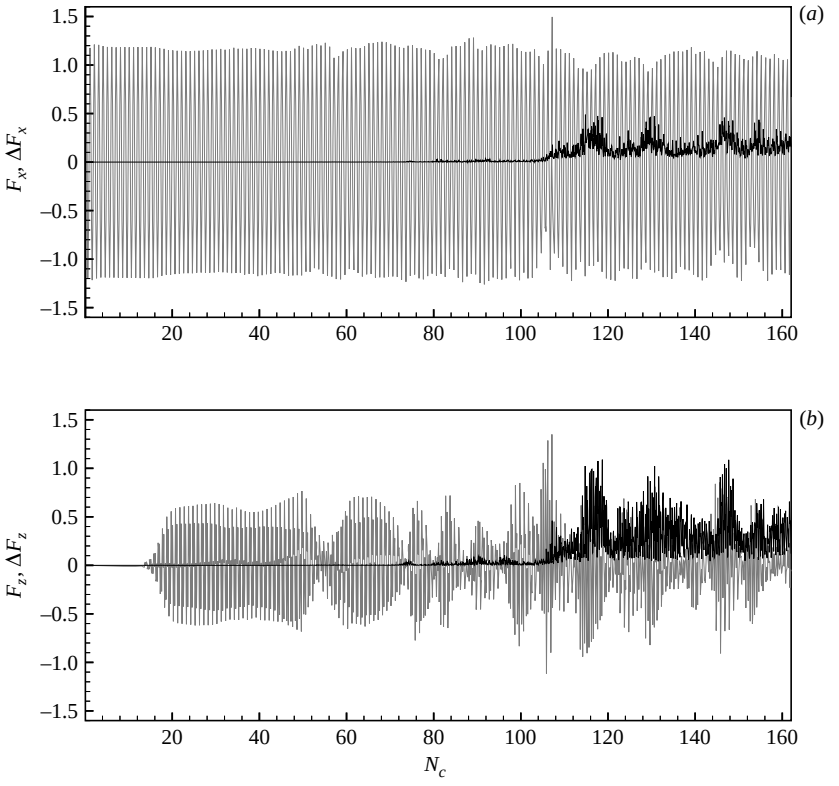

FIGURE 19. Time record of the force components (grey line) and of the maximum variation of the sectional forces $\Delta F_i(t) = F^s_{i,max} - F^s_{i,min}$ (black line): (*a*) longitudinal components; (*b*) transversal component. Regime F, $KC = 8.5$, $\beta = 20$, $Re = 170$.

axial-integrated values, appears to increase in regime F compared to regime D. This is probably due to the increased KC and Reynolds numbers. Interestingly, the fact that the maximum variation of the sectional force is always larger than the axial-integrated value now appears related not to time delay in the switching from one two-dimensional mode to the other along the axis, but to the circumferential rotation of the diagonal vortex pattern along the y-axis. This is illustrated in figure 20, which shows the time evolution of the maximum and minimum values of the sectional transversal force along the y-axis. Unlike in regime D, figure 20 shows that the sectional transversal forces oscillate in phase, because during the oscillation the sectional force maintains its sign along the axial direction. This is the evidence that a single two-dimensional mode is present along the y-axis at a certain time instant and that switching from this mode to its mirror-image occurs at the same time along y. The circumferential motion undergone by the main two-dimensional vortex structures along y, visible for example in the three-dimensional view of figure 21, is by itself thus able to produce the large variation in the sectional transversal force shown in figure 19(*b*). The typical evolution along a cycle of the transversal sectional force $F^s_z(y)$ reported in figure 22 shows the presence of a dominant mode with wavelength $\lambda = 12$, although the Fourier analysis of $F^s_z(y)$ (not given here) clearly shows that the first two modes contribute to the axial distribution of the sectional force. To be noted is that the presence of the $\lambda = 12$ axial mode is consistent with the experimental results by YR02, which

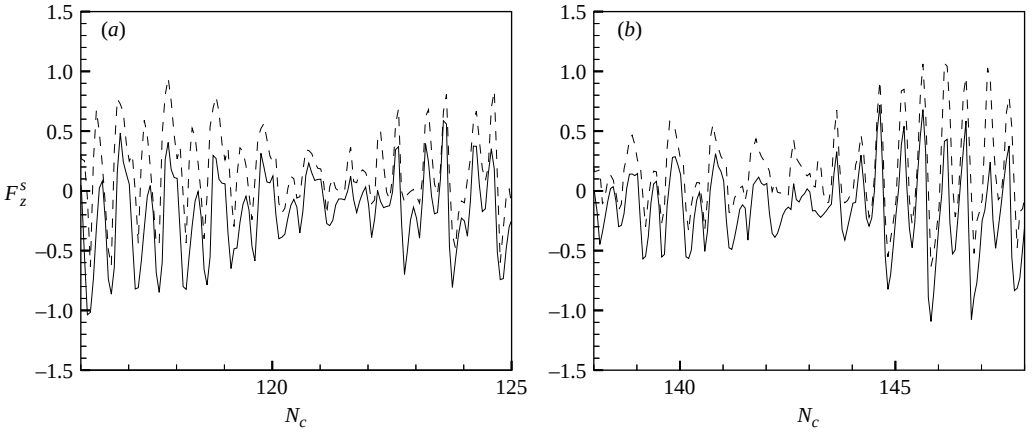

FIGURE 20. Time record of the maximum (- - -) and minimum (—) transversal sectional force F_z^s along two representative time windows of the simulation. Regime F, $KC = 8.5$, $\beta = 20$, $Re = 170$.

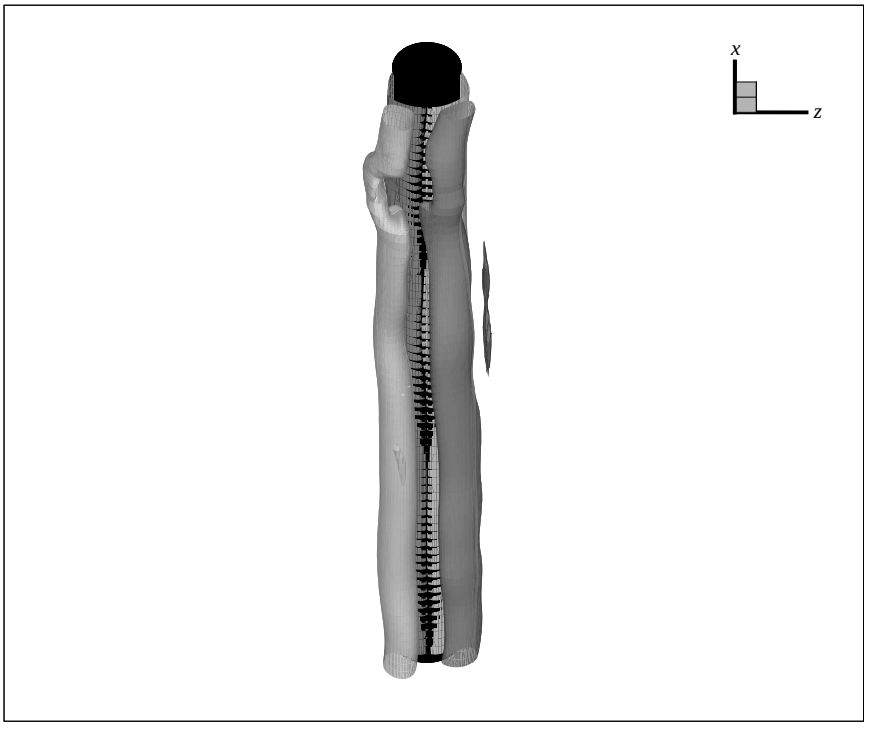

FIGURE 21. Instantaneous three-dimensional view of the vorticity ω_y near the cylinder, at the phase $t_p = 0$ of the 141st cycle. Regime F, $KC = 8.5$, $\beta = 20$, $Re = 170$.

showed the increase in the axial wave mode with KC. On the other hand we cannot exclude the presence of additional large-scale modes, although YR02 showed that for $KC < 10$ small-scale modes are mostly detected. Verification would require the use of a very long cylinder (say $L_y \geqslant 18$), beyond our present capabilities.

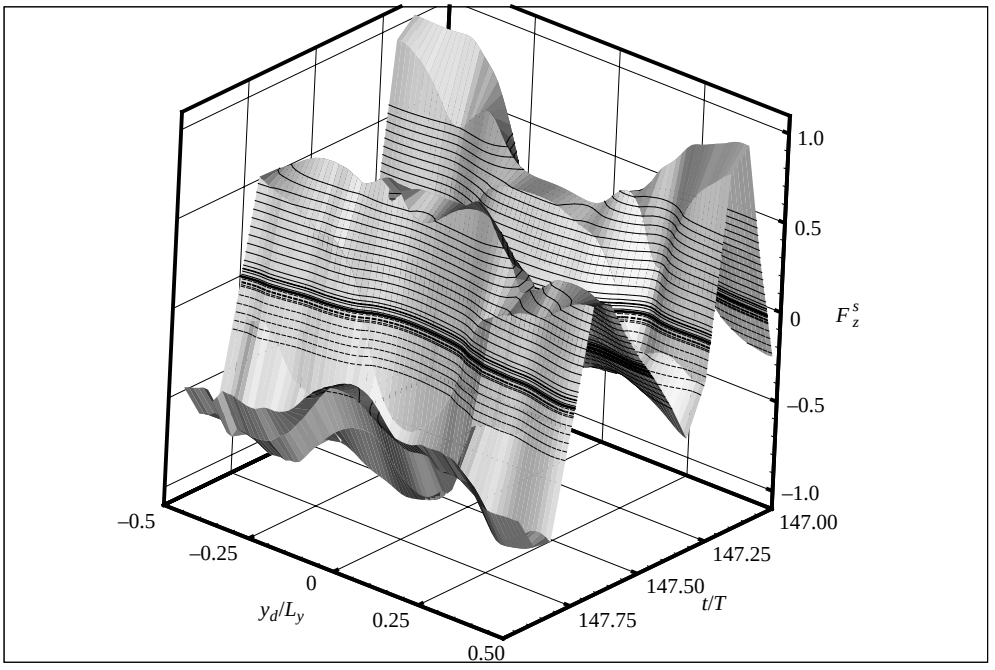

FIGURE 22. Evolution along the 147th cycle of the axial distribution of the sectional transversal force $F_z^s(y_d/L_y, t/T)$. Regime F, $KC = 8.5$, $\beta = 20$, $Re = 170$. For the coordinate system see figure 2.

5. Discussion and concluding remarks

The sinusoidal, unidirectional, oscillating flow around a circular cylinder has been investigated numerically by solving the three-dimensional and the two-dimensional unsteady Navier–Stokes equations.

Two regimes of the TB90 map have been studied: the *transverse-street* three-dimensional regime D and the double-pair *diagonal*, three-dimensional regime F. To the best of our knowledge this is the first investigation in which the three-dimensional structures visualized in TB90 have been reproduced by means of numerical simulations; the effect of three-dimensionality of the vorticity field on the axial distribution of the forces is quantified; and the results of three-dimensional computations are compared to those of equivalent two-dimensional ones.

The two-dimensional features of the flow field are not qualitatively affected by three-dimensional effects. Specifically, the asymmetric motion in the sectional planes that gives rise to the V-pattern of regime D and the diagonal pattern of regime F, as well as switching from a pattern to its mirror-image, are inherent features of the two-dimensional field. The occurrence of such vortex dynamics should be related to a two-dimensional instability in the flow field. In fact, the vortex patterns discussed above as well as their switching from one direction to the other can be simulated using pure two-dimensional models.

The three-dimensional simulation produced two main three-dimensional effects in the flow field:

(i) a circumferential motion of the main sectional vortex pattern along the y-axis. The transverse-street pattern of regime D as well as the diagonal pattern of regime F tend to be rotated around the axis of the cylinder, and the rotation can exhibit a sort

of sinuous behaviour along y, as illustrated in figure 21. In the transverse-street regime the circumferential rotation of the V-pattern is also accompanied by a variation along y of the degree of opening of the V that may degenerate into a straight line. These circumstances contribute to varying the angle of inclination of the sectional vortex pattern along y.

(ii) a time delay along y of the switching from a fundamental two-dimensional mode to its mirror-image. In other words, complete switching from one pattern to the other does not occur at the same time along the axis; rather, it appears delayed from section to section.

The experimental investigations by Obasaju *et al.* (1988) and by YR02 have highlighted the possibility that the two modes (one and its mirror image) may be present at the same time along the axis of the cylinder. The presence of the sinuous S-mode along the y-direction has been associated with this behaviour. In our computation we did not observe the simultaneous presence of the two two-dimensional modes along the axis, probably because in our investigation the Stokes number ($\beta = 20$) was much smaller than that of YR02 ($\beta = 73$) and that of Obasaju *et al.* (1988) ($\beta > 100$). On the other hand we observed that the presence of the sinuous S-mode is not necessarily associated with the simultaneous presence of the two fundamental two-dimensional modes along the axis (one and its mirror image). Indeed, the sinuous mode can also be generated by the two effects discussed above, namely circumferential motion and time delay of complete switching along the y-direction.

The effect of three-dimensional motion on the occurrence of switching is not monotonic. In regime D, three-dimensional effects tend to stabilize the presence of a certain V-pattern and the time scale of complete switching increases compared to that obtained with an equivalent two-dimensional simulation; in regime F, the opposite is true. Thus it is not possible to say *a priori* whether or not three-dimensionality acts to stabilize the presence of a particular vortex pattern. This may be due to several features, such as the type of two-dimensional vortex pattern (V-shaped rather than diagonal), or to the intensity of the fundamental two-dimensional motion in terms of the mean inclination of the two-dimensional vortex pattern with respect to the longitudinal axis.

Our results are qualitatively in good agreement with those of YR02. However, it should be pointed out that our simulations were carried out in unidirectional flow, whereas the experiments of YR02 were performed in a wavy flow, where the increase in KC was associated with a corresponding increase in the vertical motion of the fluid particles, and thus with the three-dimensionality of the external flow field. Hence it is possible to argue that most of the features observed in the experiments by YR02, such as the occurrence of the axial S-mode and the increase in the dominant axial wavelength with KC, were not related to three-dimensional forcing, because they are also observable in a unidirectional motion.

The definition of the fundamental axial wavelength λ, which can be easily detected by means of a visual analysis, gives information on the average spanwise dimension of the vortex structures present in the flow field. The visual analysis by TB90 shows that λ slightly decreases with β, is nearly independent of KC when remaining within a certain flow regime, and increases with KC for the same β when moving from regime D to regime F (compare, for example, figure 22 to figure 30 of TB90). Our results are consistent with the visual analysis by TB90, in that one observes an increase in the average wavelength with KC between regime D and regime F. These results, as discussed above, are also consistent with the finding of YR02.

Figures 22 and 30 of the visual study of TB90 show that the values of λ appear to be scattered when plotted against β for several values of KC. This may be due to the fact that those authors calculated an average value of the axial dimension of the vortex structures in cases characterized by strong variability in such wavelengths. Our computations show that, for a given couple of values of β and KC, different wave-modes may be dominant at different cycles during the simulation, making evaluation of an average wavelength very difficult. For example, figure 9 clearly shows that, although the shape of the vortex pattern in the plane $z=0$ does not change during the simulation, the axial length of such patterns varies from three to six diameters. Similar behaviour is observed in regime F.

This behaviour suggests that the average wavelength λ does not entirely determine the axial wave components present in the flow field. Indeed, the Fourier analysis shows that after the three-dimensional motion has developed, several modes make up the three dimensional distribution of the vorticity field. In particular at least three wave components appear to be dominant in each case investigated, giving rise to an appreciable variability in the wavelength λ observable in a visual analysis.

The three-dimensional flow field affects the dynamic loads induced on the cylinder. The r.m.s. value of the axial-integrated component F_x evaluated using the two-dimensional model is slightly smaller than that obtained with the three-dimensional computations. In particular the two-dimensional computations underestimate $F_{x,rms}$ by less than 1% on both regimes investigated (see table 2 and table 3). The variation in the sectional longitudinal force along the axis of the cylinder is small during the simulation. In particular, the maximum variation $\Delta F_x(t)$ amounts to about 10% and 20% respectively in regime D and regime F. Our results corroborate and extend the findings of YR02, who, on analysing the time record of the moment induced by the longitudinal force, have argued that F_x is weakly affected by three-dimensionality in the flow field.

The transversal force behaves differently from the longitudinal one. The r.m.s. value of the axial-integrated component F_z estimated with the two-dimensional mathematical model is appreciably larger than that estimated using the three-dimensional model in both regimes investigated. Specifically, in regime D and in regime F, the two-dimensional computation overestimates $F_{z,rms}$ by about 12% and 25% respectively (see table 2 and table 3). Moreover, the maximum variation in the sectional transversal force along y, namely $\Delta F_z(t) = F^s_{z,max}(t) - F^s_{z,min}(t)$, is very large and often exceeds the axial integrated value.

These effects are related to the presence of the axial sinuous S-mode, which, in the present case is generated by the circumferential motion of the sectional vortex patterns and by the time delay of switching from one pattern to the other, along the axial direction.

We have observed that the main three-dimensional effect over the induced loads consists of a small increase in the r.m.s. value of the axial-integrated longitudinal force F_x and in an appreciable reduction in $F_{z,rms}$. On the other hand, the time records of figures 6 and 16 show that the increase in the maximum of F_x from cycle to cycle is associated with a reduction in F_z and vice versa. These effects can be explained as follows. Consider the total sectional force $\boldsymbol{F}^s(y)$, whose components are respectively the already defined $F^s_x(y)$ and $F^s_z(y)$; and specifically consider the angle of inclination $\phi = \arctan F_z/F_x$ of the vector $\boldsymbol{F}^s$ with respect to the longitudinal axis. Figure 23 shows that the angle $\phi(y,t)$ varies along y from cycle to cycle at a phase position $t_p = 0.125$ at which both force components F_x and F_z are close to a local maximum in regime D as well as in regime F (see figure 6*a*ii, *b*ii and figure 16*a*ii, *b*ii). Figure 23

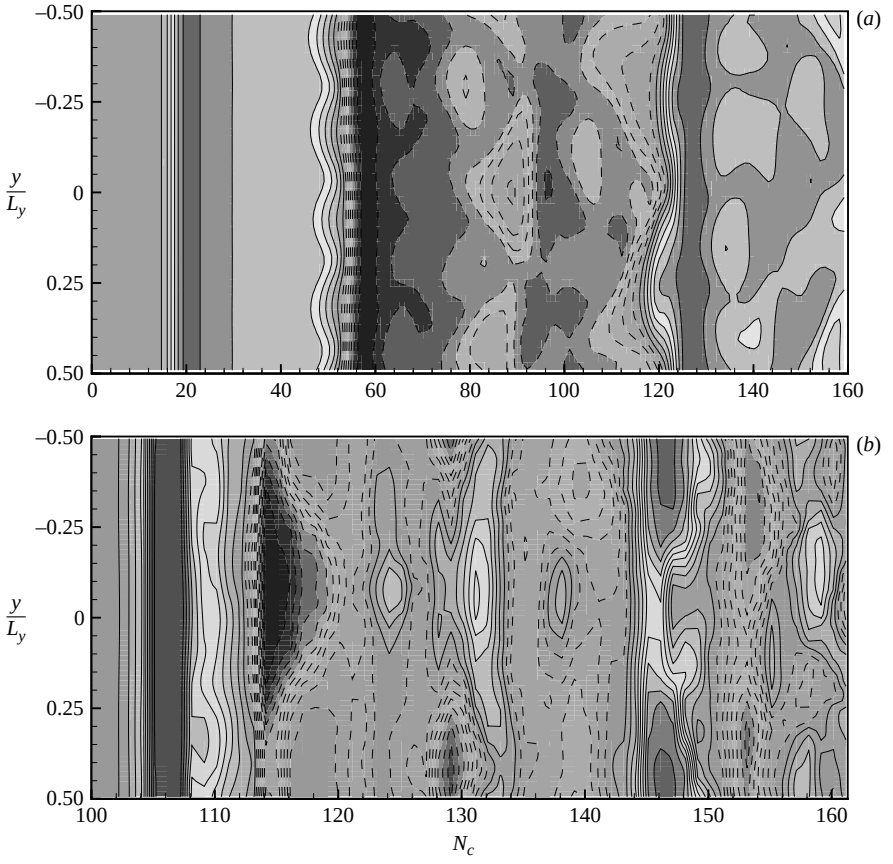

FIGURE 23. Evolution from cycle to cycle of the angle of inclination of the total force with respect to the plane $z=0$, $(\phi(y,t))$ at $t_p=0.125$: (*a*) Regime D, $KC=6.5$, $\beta=20$, $Re=130$; (*b*) Regime F, $KC=8.5$, $\beta=20$, $Re=170$. The contour levels go from $-50°$ to $50°$ for regime D and from $-35°$ to $35°$ for regime F.

shows large variations of ϕ along the y-axis, and a comparison with figure 7 and figure 17 shows that the change of sign of ϕ along y is closely correlated with the occurrence of the S-mode, the latter being detected by the change of sign of ω_y at the probe lines previously defined.

On the basis of these observations, consider a vortex pair shed in the wake of the cylinder during the oscillation. For simplicity, suppose that the intensity of the vortex pair does not change along the axial direction, and that three-dimensionality in the flow field is such as to cause a variation along the axial direction of the angle of inclination θ of the vortex pattern with respect to the plane $z=0$. The above vortex pair induces a force $\boldsymbol{F}^s(y)$ inclined by an angle $\phi(y)$ with respect to the line $z=0$, and we can assume that $\phi(y)$ is roughly equal to $\theta(y)$. The force components in the longitudinal and transversal direction will be respectively $F_x^s(y)=|F^s|\cos\phi(y)$ and $F_z^s(y)=|F^s|\sin\phi(y)$. If $\phi(y)$ is very small, we can write $F_x^s\sim|F^s|$ and $F_z^s\sim|F^s|\phi$. It follows that small variations in the angle ϕ along the y-axis, also including the change of sign of the angle itself, give rise to large variations in $F_z^s(y)$ that may exceed the axial-integrated values, and very small variations in the longitudinal component $F_x^s(y)$. The increase in the angle ϕ, still remaining confined within the range of

small-to-moderate values (ϕ about 10° to 40°), causes smaller variations in the longitudinal component compared to the corresponding variations in the transversal one. This may explain why three-dimensional effects on the longitudinal force appear to be much weaker than those on the transversal force. Moreover, the simple explanation given above shows that a reduction in the longitudinal force from cycle to cycle, which appears to be associated with a corresponding increase in the transversal one and vice versa, is basically due to the time variation in the angle of inclination of the vortex pattern and thus to the corresponding variation of ϕ.

The authors express their gratitude to Dr S. Becker of the Institute of Fluid Mechanics, University of Erlangen-Nuremberg, Germany, for the experimental data of regime A. The authors are also grateful to Professor G. Pedrizzetti of the Universitá di Trieste for making the two-dimensional (ω–ψ) code available. The research has been partially supported by the 'Ufficio per le Relazioni Internazionali' of the Universitá di Trieste, by the Université of Mostaganem, Algeria and by MIUR. The simulations were run on the SP4 supercomputer of CINECA.

REFERENCES

Armenio, V. & Piomelli, U. 2000 A Lagrangian mixed subgrid-scale model in generalized coordinates. *Flow Turbulence Combust.* **65**, 51.

Armenio, V. & Sarkar, S. 2002 An investigation of stably-stratified turbulent channel flow using large eddy simulation. *J. Fluid Mech.* **459**, 1.

Bearman, P. W. 1997 Bluff body hydrodynamics. *Proc. 21st Symp. on Naval Hydrodynamics*, p. 561.

Dutsch, H., Durst, F., Becker, S. & Lienhart, H. 1998 Low-Reynolds-number flow around an oscillating circular cylinder at low Keulegan-Carpenter numbers. *J. Fluid Mech.* **360**, 249.

Falcomer, L. & Armenio, V. 2002 Large-eddy simulation of secondary flow over longitudinally-ridged walls. *J. Turbulence* **3**, 008.

Honji, H. 1981 Streaked flow around an oscillating circular cylinder. *J. Fluid Mech.* **107**, 509.

Justusen, P. 1991 A numerical study of oscillating flow around a circular cylinder. *J. Fluid Mech.* **222**, 157.

Kuhtz, S. 1981 Experimental investigation of oscillatory flow around circular cylinders at low β numbers. PhD thesis, University of London.

Obasaju, E. D., Bearman, P. W. & Graham, J. M. R. 1988 A study of forces, circulation and patterns around a circular cylinder in oscillating flow. *J. Fluid Mech.* **196**, 467.

Pentek, A., Kadtke, J. B. & Pedrizzetti, G. 1998 Dynamic control for capturing vortices near bluff bodies. *Phys. Rev.* E **58**, 1883.

Sorenson, R. L. 1980 A computer program to generate two-dimensional grids about airfoils and other shapes by the use of Poisson's equations. NASA TM 81198. NASA Ames Research Center.

Tatsuno, M. & Bearman, P. W. 1990. A visual study of the flow around an oscillating circular cylinder at low Keulegan-Karpenter numbers and low Stokes numbers. *J. Fluid Mech.* **211**, 157 (referred to herein as TB90).

Williamson, C. H. K. 1985 Sinusoidal flow relative to circular cylinders. *J. Fluid Mech.* **155**, 141.

Yang, Y. & Rockwell, D. 2002 Wave interaction with a vertical cylinder: spanwise flow patterns and loading. *J. Fluid Mech.* **460**, 93 (referred to herein as YR02).

Zhang, J. & Dalton, C. 1999 The onset of three-dimensionality in an oscillating flow past a fixed circular cylinder. *Intl J. Numer. Meth. Fluids* **30**, 19.

Zang, Y., Street, R. L. & Koseff, J. R. 1994 A non-staggered grid, fractional step method for time-dependent incompressible Navier-Stokes equations in curvilinear co-ordinates. *J. Comput. Phys.* **114**, 18.